Susitna-Watana Hydroelectric Project
(FERC No. 14241)

Fluvial Geomorphology Modeling below Watana Dam
Study Plan Section 6.6

2014-2015 Study Implementation Report
Attachment 1, Appendix B

FA-128 2-Dimensional Sediment-transport Model Development and Calibration

Prepared for

Alaska Energy Authority

SUSITNA-WATANA HYDRO

Clean, reliable energy for the next 100 years.

Prepared by

Tetra Tech Inc.

October 2015

TABLE OF CONTENTS

LIST OF TABLES

LIST OF FIGURES

1. INTRODUCTION

As part of the Fluvial Geomorphology Modeling below Watana Dam Study (Study Plan Section 6.6), 2-dimensional (2-D) sediment-transport modeling (also referred to as bed evolution modeling in some documents) will be conducted *to assess the potential effects of the Susitna-Watana Hydroelectric Project on the dynamic behavior of the river downstream of the proposed dam, with particular focus on potential changes in instream and riparian habitat*. The Project will alter flow rates and sediment supply downstream of the dam and the channel form is expected to respond to the changes, which in turn, will alter future instream and riparian habitat conditions.

Attachment 1 of the Study Implementation Report (SIR) for Study 6.6 is the 2014 Fluvial Geomorphology Model Development Technical Memorandum for the initial 1-D and 2-D bed evolution models. This appendix to Attachment 1 describes the development and calibration of the 2-D bed evolution model (BEM) for Focus Area 128 (FA-128, Slough 8A). This is an extension of the earlier proof-of-concept exercise (Appendix A of Tetra Tech 2014a) where a detailed 2-D hydraulic model of FA-128 (Slough 8A) was developed, calibrated, and applied over a wide range of flows to provide input to the aquatic habitat analyses of Study 8.5.

The 2-D sediment-transport model was developed for FA-128 (Slough 8A) (Figure 1-1) to evaluate local scale issues. Local scale issues are generally defined on the scale of the habitat and geomorphic features within the focus areas. The 1-D sediment-transport model (referred to as the 1-D bed evolution model) was developed to evaluate the reach based issues (Appendix A).

A 2-D sediment-transport model of FA-128 (Slough 8A) was developed using measured bed-material gradations, bathymetric and topographic survey data collected in 2013 and LiDAR data collected in 2011; this geometry represents the existing (Year 0) conditions. The hydraulic portion of the model was calibrated to measured water-surface elevations, flow measurements and velocity data collected as part of ISR Study 8.5. For the sediment-transport modeling, input sediment transport versus discharge rating curves were developed for the existing and with-Project (Max LF OS-1b) conditions based on output from the 1-D sediment-transport model. Representative surface and subsurface bed-material gradations were developed and applied to the represent the existing conditions.

2. 2-D MODEL DEVELOPMENT AND CALIBRATION

2.1. Model Description

The modeling was conducted using SRH-2D Version 3 software developed by the Bureau of Reclamation (USBR). SRH-2D is a finite-volume, hydrodynamic and sediment-transport model. The hydrodynamic portion of SRH-2D computes water-surface elevations and horizontal velocity

components for sub-, super-, and trans-critical free-surface flow in 2-D flow fields. The SRH-2D mesh for FA-128 (Slough 8A) was developed with Version 11.1 of the Aquaveo Surface Water Modeling System (SMS) graphical user interface (Aquaveo 2013).

SRH-2D computes bed elevation change (scour and deposition) by simulating the interaction between sediment transport and the hydraulics of the flow. The model simulates both vertical changes in bed elevations and the associated changes in surface bed-material gradation. In general, the bed elevation changes are simulated by estimating the bed-material transport capacity in each element based on the flow hydraulics and bed-material characteristics, comparing the estimated capacity with the sediment supply from adjacent elements, and adjusting the bed elevations to account for the differences between the supply and the transport capacity (i.e. the net addition or loss of sediment to the area within the element). SRH-2D routes the sediment through the reach by size-fraction; thus, model results reflect changes in the bed-material gradation that result from differences between the supply and transport capacity of the individual size fractions. This capability allows the model to simulate fining and coarsening of the bed surface in response to changes in hydraulic conditions and upstream sediment loads. SRH-2D contains an unsteady total load algorithm that automatically partitions "suspended load, bed load or mixed load depending on the transport model parameter of local flow hydraulic" (Greimann et al. 2008).

SRH-2D uses a flexible mesh composed of triangular and quadrilateral elements which allows the resolution of the computational elements to vary throughout the model domain, which provides a significant advantage over models with a structured mesh (e.g. the orthogonal mesh used by CCHE2D and MD_SWMS) because the density of the computational points can be increased in areas with large topographic variability and areas of special interest, while a lower resolution can be used in other areas to maintain reasonable model size and computational efficiency.

Two versions of SRH-2D were used for the sediment-transport modeling that have build dates of May 2013 and October 2014. The hydrodynamic and sediment-transport routines in both versions are consistent. The October 2014 version has additional features related to the sediment-transport modeling, including improved functionality to restart a model. Both versions have the ability to restart a simulation using the hydrodynamic conditions from a previous run. However, the October 2014 version has the added capability of being able to retain the predicted bed-material characteristics from a previous simulation. This is considered an important improvement in the model capabilities because an initial run can be used to establish bed-material gradations throughout the channel network that are used as the starting condition for other runs. This warm-up procedure avoids the initial large change in bed elevation by generating gradations for the individual elements that are more consistent with the hydraulics. A typical warm up model may be run for a year or longer.

2.2. Hydraulic Model Development

The 2-D sediment-transport model was developed using the same procedures and data that were used to develop the 2-D hydraulic model (Tetra Tech 2014a). The primary difference is that the sediment model has a coarser resolution than the hydraulic model. The coarser resolution is partially due to the limited number of elements available for sediment modeling and because the sediment model is run for extended durations of unsteady flows rather than steady state conditions the hydraulic model is run. The hydraulic model's finer mesh provides the spatial resolution, as fine as 2m, identified for elements of the aquatic habitat analysis to be conducted by the Fish and Aquatics Instream Flow Study (Study 8.5). The model parameters (e.g. Manning's *n*-values, turbulence model, boundary conditions) applied to the 2-D hydraulic model were also applied to the sediment-transport model.

2.2.1. Topographic Data

The topography of the focus area (channel and overbank) is represented by elevations assigned to each node in the mesh. The bathymetric and topographic survey data collected for Study 8.5 (Figure 2.2-1) and the Indexed 2011 Mat-Su LiDAR data reported in Study 6.6 were used to develop a Triangular Irregular Network (TIN) (Figure 2.2-2). The TIN was used to assign elevations to the mesh nodes.

The horizontal datum for the surveys and models are referenced to the State Plane Coordinate System, North American Datum of 1983 (NAD83) (Alaska, Zone 4) and the vertical datum is the North American Vertical Datum of 1988 (NAVD88).

The mesh was constructed to extend up- and downstream of the focus area boundary and to extend between the valley walls (Figure 2.2-3). The mesh was extended approximately 300 feet downstream of the focus area boundary to provide better prediction of the flow distribution between the main channel and side channel near the downstream boundary. The mesh also was extended approximately 2,000 feet upstream of the focus area to provide better prediction of the velocity distribution at the upstream boundary of the focus area and to better represent the flow split into the side channel located near the left (east) boundary of the model.

The number of elements in the mesh in earlier versions of sediment-transport module of SRH-2D was limited to approximately 16,000 elements. The two versions of SRH-2D used in this study do not have a mesh size limitation; however, for practical purposes, the 16,000 element mesh provides a good balance between computational efficiency and topographic resolution, and therefore, was used as a target size during mesh development.

The mesh resolution was varied using smaller elements in topographically variable areas and larger elements in areas with low topographic variability (e.g. overbank areas) (Figures 2.2-3 and 2.2-4). The typical side length of the triangular and trapezoidal elements in the main and side channels is approximately 40 feet wide by 50 feet long. In side and upland sloughs the element dimensions

generally range from 10 to 40 feet. The overbank elements are typically comprised of triangular elements ranging in size from 25 to 130 feet, with a representative size of approximately 75 feet. The resulting mesh is 11,300 feet long and contains 16,843 elements and 12,050 nodes.

A quality control check of the mesh was conducted using the "mesh quality" option in SMS (Aquaveo 2013). The mesh quality check included a review of the change in area between adjacent elements (no more than 50 percent), number of connecting elements (no more than 8) and the minimum and maximum element angles (10 and 130 degrees, respectively). Due to differences in sizes between adjacent elements, particularly in areas of large topographic change (e.g. between the channel and the overbank), approximately 100 elements exceeded the "element area change" parameters. This is a very small proportion of the total elements (<1 percent) is not a concern especially since this is a finite volume model. The mesh is of very good quality for the purposes of sediment-transport modeling.

2.2.2. Material Roughness Properties

SRH-2D uses Manning's *n*-values to define boundary friction losses and a turbulence model (parabolic or k-ε) to compute the energy losses due to internal turbulence. Six different roughness material types were used to represent the channel, islands and various overbank surfaces and vegetation zones (Figure 2.2-5). The roughness zones were developed based on the geomorphic mapping, aerial photography and field observations. The overbank roughness ranged from 0.08 for lightly vegetated areas to 0.17 for overbank areas with thick vegetation. Main channel, side channel and sloughs were assigned a Manning's *n*-value of 0.03 and 0.04 based on field observations, similar experience with other rivers, and standard references (Chow 1959; Barnes 1967; Hicks and Mason 1991; Julien 1995). A parabolic turbulence model was used to calculate internal turbulence and a value of 0.7 was used based on previous calibration efforts (Tetra Tech 2014a).

2.2.3. Downstream Boundary Conditions

The downstream boundary conditions for the model consist of a specified water-surface elevation for the particular discharge that is being modeled. A stage versus discharge rating curve was developed from measured water-surface elevations collected over a range of flows and using predicted values from the 1-D model. The measured water-surface elevations used to develop the rating curve were located near the downstream boundary, but not at the boundary (Figure 2.2-6). Therefore, it was necessary to translate the measured values downstream using a slope approximation to determine the water-surface at the boundary. The six blue squares on Figure 2.2-6 represent the measured water-surface elevations, and therefore vary slightly from the rating-curve based on the small difference in location. The minimum elevation on the curve represents the channel thalweg.

2.2.4. Other Model Parameters

For model validation purposes, the hydrodynamic portion of the model was run using a 5-second time step at a constant discharge for 48 hours. This period was sufficiently long to ensure the model reached steady-state conditions.

Monitor lines and monitor points were input to the model to evaluate the hydraulic, sediment-transport and bed-material characteristics at specified locations. A "monitor" line is a modeling option in SRH-2D used to compute flow and sediment flux across a line that is defined by connecting a series of mesh nodes. Monitor lines were located at each of the ADCP transects in order to make comparisons between the measured and predicted flows (Figure 2.2-7). Monitor points were specified at areas of interest which include water-surface elevation measurement locations, bed-material measurement locations, and near the up- and downstream boundaries of the model (Figure 2.2-7). Water surface elevations were surveyed during the ADCP measurements and when bathymetry was surveyed. When the ADCP data was collected, water surface elevations were surveyed at the endpoints of the ADCP transects. When the bathymetry was collected, numerous water surface elevations were collected in the area along the water edge. These data are shown in Figure 2.2-8.

2.3. Model Validation

Because the coarser sediment model was set up using the same hydraulic parameters (roughness and turbulence) as the very detailed calibrated hydraulic model, the hydraulics of the sediment model were not specifically calibrated, but were validated as comparable to the detailed model. The model was run using the previously detailed model parameters (Tetra Tech 2014a) and was validated to discharge measurements, velocity (magnitude and direction) measurements and to water-surface elevations measurements.

2.3.1. Validation Data

Acoustic Doppler Velocity Profiler (ADCP) measurements were collected at FA-128 (Slough 8A) on July 2, 2013, and September 10, 2013, when the discharge in the river was 24,705 and 26,124 cfs, respectively (Table 2.3-1). The ADCP data were used to calculate the discharge at transects and to calculate the depth-average velocities.

The ADCP data were collected across transects (i.e. perpendicular to the main flow direction) and longitudinally (i.e. parallel to the river) (Figure 2.2-7) as part of ISR Study 8.5. In Figure 2.2-7, transects are labelled with a "T" and the longitudinal profiles are labeled with an "L". Typically, repeat ADCP measurements were conducted at transects in the main channel as part of the quality control procedures implemented to ensure accurate flow measurements (Study 8.5). The ADCP flow measurements conducted on July 2, 2013, and September 10, 2013, are reported in Study 8.5.

Depth-averaged velocities were calculated from the raw ADCP measurements using the RiverSurveyor Live (Version 3.7) (Sontek/YSL 2013) software.

The model was also validated to available water-surface elevation measurements collected on 4 occasions over a range of flows from 20,500 to 26,124 cfs (Figure 2.2-8; Table 2.3-2). Water-surface elevation (WSE) measurements were collected concurrently with the ADCP measurements and therefore the corresponding discharges are known. The discharges associated with the water-surface elevation measurements collected July 24 and 26, 2013, were calculated using the following procedure:

1. A Project River Mile (PRM) was calculated to the nearest 0.1 mile for each WSE measurement.
2. The travel time for each WSE measurement was determined based on travel times (reported in ISR Study 8.5, Part A, Appendix C) between the Gold Creek gage (USGS Gage #15292000) located at PRM 140 and the focus areas (Figure 2.3-1).
3. A discharge for each WSE measurement was calculated based on the time of the measurement, the travel time from Gold Creek, and the 15-minute interval discharge measurements at the Gold Creek gage.

2.3.2. Model Validation Results

The hydrodynamic portion of the model was run using the previously detailed model parameters, which included Manning's *n* roughness value of 0.03 for the main channel and 0.04 for the side channels (Figure 2.2-5), at discharges of 26,124 cfs (10-Sep-2014), 24,705 cfs (2-Jul-13), 20,132 cfs (24-Jul-13) and 20,500 cfs (26-Jul-13) (Table 2.3-2).

A comparison of the measured and predicted water-surface elevations at 26,124 cfs shows very good agreement (Figure 2.3-2; Table 2.3-2). In Figure 2.3-2, the bars indicate the relative differences in water-surface elevations in the direction of the error. For example, if the bar is in the lower half, then the predicted water-surface elevation is lower than the measured values. Conversely, if the bar is in the upper half, then the model is over predicting the water-surface elevation. Green bars indicate differences of less than 0.5 feet, orange bars indicate differences between 0.5 and 1 feet, and red bars indicate differences greater than 1 foot.

The differences between the measured and predicted water-surface elevation at a 26,124-cfs range from -0.6 to 0.2 feet, with an average difference of -0.3 feet, indicating the model is slightly under predicting the water-surface elevation across the focus area (Table 2.3-2). The largest differences occur at the confluence of a side channel and side slough and can been seen slightly to the left of center of Figure 2.3-2. It should be noted that areas that appear to have disconnected water surfaces, especially Slough 8A along the middle-right area of the figure, are connected by single elements. The software only fills areas that have at least two adjacent wet elements.

The predicted flow distributions match the measured values well (Table 2.3-3). In the larger channels (those conveying at least 20 percent of the total flow), the differences are less than 5

percent. In the smaller channels, the differences are larger. Because the flow splits are typically only a few percent of the total flow, it is expected that larger relative differences will occur in the smaller channels. For example, at T2B, the predicted value is 285 cfs compared to the measured value of 250 cfs, a 14-percent difference between the values, but each represents very nearly 1 percent of the total flow. At T7, the predicted value is 4.8 cfs compared to the measured value of 3.7 cfs, a 31-percent difference; considering that this is a 1.1 cfs difference in a very small split-flow area this is a very good result at T7.

Discharge measurement error is another factor in the calibration of the model because measurements may contain errors and the total flow in the river is changing over the measurement period of several hours. Continuity is not always preserved in the measurements, which limits model calibration. For example, T3C minus T2D should equal T2B plus T2C because these flows split off between the two main channel locations. In the July 2, 2013, measurements, T3C-T2D=703cfs and T2B+T2C=1,002 cfs, producing a continuity difference of 299 cfs for these locations. The model must maintain continuity and computes 1,053 cfs for this simulation. The 299-cfs difference in the measurements is comparable to the larger differences between the model and measurements. The same comparison for the September 10, 2013, measurements produces a 175-cfs difference (1,309 cfs versus 1,134 cfs) compared to the model result of 1,230 cfs. For these locations the measurement inconsistencies of 175 and 299 cfs represent unavoidable model versus measurement differences.

Comparisons of the predicted and measured velocity magnitudes along the transects show very good agreement (Figures 2.3-3 through 2.3-17). Where there are repeated ADCP transects, two model transects are included representing the different tracks. The agreement is good especially considering the measured velocity data show significant variation along the ADCP transects. For example, repeat ADCP measurements were collected at T1A and T1B (Figures 2.3-3 and 2.3-4, respectively) which show variation in the measured velocities of up to 3 ft/s. This is expected given the highly turbulent flow conditions and that the ACDP captures near-instantaneous values relative to the model, which does not directly include temporal turbulent structure. In general, the predicted velocity distributions fall within the scatter of the measured data. The predicted velocity distributions match better in the larger channels compared to the smaller side channels. Following are some comparisons of selected transects.

- At T1A (Figure 2.3-3), the predicted velocities are slightly higher along the left side of the channel and slightly lower to the right of center compared to the measured values.
- T2D (Figure 2.3-8) shows very good agreement between the measured and predicted velocities.
- T6 and T7 (Figures 2.3-16 and 2.3-17, respectively) transects are located across smaller channels. At T6, the predicted velocities match the measured data well. At T7, the predicted velocities are approximately 0.2 ft/s lower than measured velocities.

- The correlation (R^2 value) between measured and predicted velocity magnitudes is 0.87 (Figure 2.3-18) which indicates very good agreement. Pasternack (2011) suggests an R^2 value in the range of 0.4 to 0.8 indicates good calibration. The average difference in the velocities (predicted-measured) is 0.09 ft/s indicating the model, on the average, is slightly over-predicting the velocities at the measured transects.

Comparisons of the predicted and measured velocity magnitudes and directions are shown in planform view for a series of selected transects (Figures 2.3-19 through 2.3-25). The direction of the velocity vectors and the velocity magnitude match the measured values well.

Comparison of the predicted flow distributions at 24,705 cfs (July 2, 2013) match the measured values well (Table 2.3-4). In the larger channels that include at least 20 percent of the total flow, the differences are less than 5 percent. In the smaller channels, the differences are larger, but are similar in scale to the September 10, 2013, measurements. Comparison of the differences in water-surface elevations (predicted-measured) at 24,705 cfs (2-Jul-2013) show that the model, on the average, is under predicting the measured water-surface elevation by approximately 0.1 foot (Figure 2.3-26; Table 2.3-2).

At discharges of 20,132 cfs (July 24, 2013) and 20,497 cfs (July 26, 2013), the model predictions are in good agreement with the measured values (Table 2.3-2). On average, the model is over predicting the water-surface elevation by less than 0.1 and 0.3 feet, at 20,132 and 20,497 cfs, respectively. At 20,497 cfs, the largest differences occur at measurements collected along Slough 8A, which skews the average to be slightly high. Over the four modeled flows, the average difference in water-surface elevations is -0.01 feet and a RMS error of 0.43 feet, indicating the model is well validated over a range of flows from 20,132 to 26,124 cfs (Table 2.3-2).

3. SEDIMENT-TRANSPORT MODELING

To perform the sediment-transport modeling, the hydrodynamic portion of the model was modified by incorporating the required sediment-transport parameters, which include the sediment-transport equations, representative bed-material gradations and discharge versus sediment-transport rating curves. Sediment-transport rating curves were developed to represent the sediment input to the Susitna River and Skull Creek under existing and with-Project conditions (Max LF OS-1b scenario).

3.1. Bed-material Gradations

The bed material is represented in the model as a material type. Each material type, except for the "non-erodible" material, is assigned a representative surface and subsurface gradation. The spatial distribution of the material types was selected based on field observations, aerial photography and the bed-material mapping (R2 2014). Three material types were assigned to represent the Susitna River, two material types to represent Skull Creek and a "non-erodible" material to represent the

overbank areas and vegetated islands (Figures 3.1-1 and 3.1-2). Sediment can deposit on a non-erodible material, and later erode, but not below the initial elevation.

Due to the hydraulic conditions (velocity, depth and turbidity) in the river, it was not possible to measure the bed material in the wetted areas during the summer season. Winter time bed-material sampling was conducted along the main channel. Measurements collected along the Middle River (Tetra Tech 2014b) (Figure 3.1-3) were used to develop a representative surface gradation for Material 1, which has a median (D_{50}) size of 100 mm.

Material Types 2 and 3 were developed based on 13 surface and 5 subsurface measurements collected in the vicinity of FA-128 (Slough 8A) (Figure 3.1-4). The samples were collected at the head of bars and on bars located along the side channels. The representative median size (D_{50}) of the surface material is 54 mm (Figure 3.1-5) and the median size of the subsurface samples is 32 mm (Figure 3.1-6).

The bed-material mapping conducted as part of ISR Study 8.5 (R2 2014) indicated areas of bedrock and cobble-to-boulder sized material. The bed-material gradation for the boulder-sized material (Material 4) was developed by shifting the Material 2 curve until the median size of the gradation was 256 mm (the dividing line between boulders and cobbles). Material 5 represents the non-erodible material type which includes areas of bedrock, vegetated islands and the overbank areas. The measured subsurface gradation (Figure 3.1-6) was applied as the subsurface layer to Materials 1, 2, 3 and 4.

At Skull Creek, the September 2013 flood caused significant deposition in the vicinity of the railroad bridge. A large portion of the deposited material was excavated and moved by Alaska Railroad to maintain conveyance through the bridge opening, which resulted in a chute type channel with berms on both sides of the channel that extend from upstream of the bridge to the confluence with the Susitna River. The excavated material (Material 6) has a median size (D_{50}) of 23 mm. The bed-material gradation of the armored channel bed has a much coarser median size of 69 mm (Material 7). The gradation of Material 6 was applied as the subsurface gradation for Materials 6 and 7 (Figure 3.1-2).

3.2. Sediment-transport Equations and Sediment Discharge Rating Curves

Sediment-transport equations were selected to estimate the sediment-transport capacity in the Susitna River and Skull Creek. Discharge versus sediment-transport rating curves were developed for the existing and with-Project conditions to input sediment into the models at the upstream boundary of the Susitna River and at Skull Creek.

Under existing conditions, the Susitna River transports a significant amount of fine sediments in the silt-to-sand sized range that are primarily derived from glacial processes. Sediment-transport measurements conducted by the USGS indicate these finer sediments are primarily transported as

suspended material. The channel bed and tributaries are comprised mostly of gravel- to boulder-sized material which is primarily transported as bed load. Due to the lack of appropriate sediment-transport equation to represent the wide range from sand- to boulder-sized material, it was necessary to select two sediment-transport equations that are applied simultaneously in SRH-2D. The Engelund-Hansen (1967) total-load equation was selected to estimate the sediment load for the sand-sized material (0.0625 to 2 mm) and the Wilcock-Crowe (2003) bed-load equation was selected for gravel- to boulder-sized material (2 to 512 mm). As mentioned previously, SRH-2D contains an unsteady total load algorithm that automatically partitions suspended load, bed load or mixed load depending on the transport model parameter of local flow hydraulic (Greimann et al. 2008).

In SRH-2D, the sediment supply to the model is specified using a user-defined input sediment-rating curve, a sediment-transport hydrograph, or the "capacity" option that estimates the supply based on the transport capacity at the upstream boundary. No sediment-transport measurements were available within the focus area to directly develop a sediment-rating curve or a sediment inflow hydrograph. Because the bed of the channel is composed of cobble- to boulder-sized material and the sediment supply to the reach is primarily sand-sized material, the capacity option predicted unrealistically low supply rates for the sand-sized material. As a result, sediment-transport versus discharge rating curved were developed for the Susitna River using output from the 1-D sediment-transport model (HEC-RAS). A sediment-transport rating curve for Skull Creek was developed by estimating the sediment-transport loads predicted by Parker's (1990) bed-load equation using hydraulic output from the Skull Creek hydraulic model (HEC-RAS) and measured bed-material gradations.

The sediment-rating curves require sediment-transport rates for each size fraction for a range of modeled flows. Both the Susitna River and Skull Creek gradations were represented by nine size classes; two classes to represent the sand-size material (0.0625 to 0.25 and 0.25 to 2 mm), five gravel classes (2 to 4, 4 to 8, 8 to 16, 16 to 32, and 32 to 64 mm) and two classes to represent the cobble- to boulder-sized material (64 to 128, and 128 to 512 mm).

The 1-D model was run over a 50-year period (see Appendix A of Attachment 1) for Existing and Max LF OS-1b conditions. The first 10 years of the of the 1-D model simulation was considered as the warm-up period and was not used to develop the rating-curves. The sediment-rating curves for the Susitna River were developed from the 1-D (HEC-RAS) model output at PRM129.7; this cross section is located approximately 2,000 feet downstream of the 2-D model upstream boundary. The sediment-transport rates at this cross section were considered representative of the sediment load to the 2-D model.

The sediment rating curves were developed using a "binning" method as opposed to the more traditional method of applying a power-fit regression line through the predicted transport rates. The binning approach was used to maintain a more consistent amount of data over the flow range. A comparison of the binning and trendline methods for the existing conditions showed that both

methods yielded very similar results (Figure 3.2-1). However, for the Max LF OS-1b conditions, there is significantly more scatter in the data and the regression line method was under-predicting the sediment-transport rates (Figure 3.2-1).

The sediment-rating curves were developed using the following binning method:

1. The predicted sediment-transport rates from the HEC-RAS model were separated into the 9 size classes.
2. For each size class, the discharges within a specified range (e.g. ±500 cfs) were binned into 10 classes ranging from 8,000 to 60,000 cfs. For example, for the 10,000 cfs bin, all the discharges in the range of 9,500 to 10,500 cfs were assigned to that bin. For the lower discharge bins, there were many values in each bin; however, for the higher discharge bins, there were significantly fewer values in each bin due to the infrequent high flows, and it was necessary to increase the range. For example, for the 60,000 cfs bin, the range increased to ±2,000 cfs to ensure sufficient values in the bin.
3. The average sediment-transport rates for each discharge bin and for each size class were calculated.
4. The resulting sediment-transport rates were used to develop discharge versus sediment-transport rating curves for each size fraction.
5. A discharge versus sediment-transport rating curve was also developed for the total sediment load using the same methodology.
6. Regression equations were developed for the 9 size class rating curves and for the total sediment load. The regression equations were used to extend the rating curves between 1,000 and 7,000 cfs and between 60,000 and 70,000 cfs.
7. A check was made to ensure for each discharge, the sum of sediment-transport rates predicted by the 9 rating curves matched the total load rating curve. In cases where they did not match, the sediment-transport rates for each of the 9 size classes were scaled to make them match the total load. In all cases, the sediment-transport rates were scaled by no more than 2 percent.

A comparison of the rating curves for the total load shows that the total sediment load is approximately 2 to 3 orders of magnitude larger under existing conditions compared to with-Project conditions (Figure 3.2-1). This is primarily due to the significant decrease in the sand load under with-Project conditions (Figure 3.2-2). Under with-Project conditions there is significantly more relative scatter in the predicted sand loads (at a discharge of 10,000 cfs sand loads generally ranging from 0.2 to 200 tons/day, an absolute difference of 200 tons/day and a relative factor of 1,000) but there is considerably more absolute scatter for existing conditions (500 to 1,000 tons/day, an absolute difference of 500 tons/day and a relative factor of 2 for the same discharge). For existing conditions the sand concentrations range from 10 to 2,000 ppm, showing a considerable flow dependency, but and for with-Project conditions the sand concentrations infrequently exceed 10 ppm and less than 1 ppm approximately half the time, showing near clear-water flows for the entire flow range.

In contrast to the sand-load rating cures, the predicted gravel loads rating curves are similar to each other under existing and with-Project conditions (Figure 3.2-3). The rating curve for the with-Project conditions indicates a slight increase in sediment-transport loads compared to the existing conditions. The increase may be due to the lack of data at higher flows under the with-Project condition and due to extrapolating the rating curve, although some of the highest points are from the with-Project run. It may also be that there is more availability of gravel for the with-Project condition because the quantity of gravel stored at low flows may be more available at the infrequent high flows. This will be investigated further as part of the final 1-D BEM development. Because the gravel-transport loads are low under both existing and with-Project conditions, and that the higher discharges occur very infrequently under with-Project conditions, these differences are likely to have minor effects on the modeling results. Cumulative gravel load is lower (less than half) for with-Project conditions because flows and gravel supply are decreased. Gravel concentrations are rarely greater than 10 ppm for either condition.

The sediment-rating curve for Skull Creek was developed by applying Parker's (1990) surface-based bed-load equation with the hydraulic output from a 1-D model (HEC-RAS) of Skull Creek and a representative bed gradation. The geometry for the HEC-RAS model was developed using cross-section survey data collected by Tetra Tech in August 2013. Roughness values (Manning's *n*-values) for the main channel vary with discharge based on estimates using Jarrett's (1984) equation and range from 0.08 to 0.14 over the range of modeled flows. A constant *n*-value of 0.15 were used to represent the overbank areas. The model was run for a range of discharges from 10 to 200 cfs and the model output was used to develop reach-averaged values (hydraulic depth, velocity and slope).

Parker's (1990) equation was used to predict the sediment-transport rates for sizes present in the measured surface gradation, which included 4 mm sizes and larger. Parker's approach excludes sizes less than 2 mm (sand sizes). To account for the sand sizes an additional 16 percent was included to represent the fraction in the subsurface gradation. This left the 2 to 4 mm size unrepresented, which was not present in the surface gradation but represented 7 percent of the subsurface. In the final modeling, if a size greater than 2 mm is not sampled in the surface material, it will either be included as part of the Parker equation application, or it will be included as part of the sand adjustment. The resulting sediment-rating curves are shown in Figure 3.2-4. The rating curves were applied for the existing and with-Project conditions simulations. The loads are high for the lower discharges, but may be representative based on the very steep channel (0.025 slope). In the final tributary loading evaluation, the suitability of other transport formulas will be evaluated.

3.3. Flow Hydrographs

Hydrologic input to the model consists of an unsteady flow time-series that were developed for the Susitna River to represent existing and Max LF OS-1b conditions, and for Skull Creek. The flows for Skull Creek are the same for existing and with-dam conditions.

Hourly flows were developed by Study 8.5 (ISR Appendix K) for the Susitna River and Skull Creek for the 60-year period from WY1950 to WY2010. Three annual hydrographs were selected to represent the Wet (1981), Average (1985) and Dry (1976) years (ISR Study 8.5 Appendix J). In general, the annual flow hydrographs for the existing conditions consist of an initial long-base flow period from approximately Day 0 to Day 210, followed by a significant increase in flows over the summer months from approximately Day 210 until the end of the Water Year.

To reduce the model simulation time, the majority of the base flow period was not modeled. The simulation period starts near the end baseline-flow period for existing conditions when the flows in the Susitna River are less than 10,000 cfs and extend for 3,100 hours (129 days). At the end of the simulations period, the flows in the Susitna River for the Wet-, Average- and Dry-year hydrographs are less than 15,000 cfs. The representative Max LF OS-1b hydrographs cover the same periods as the existing conditions.

For the Susitna River, the peak flows for the existing conditions for the Wet, Average and Dry years are 64,940, 41,640 and 35,470 cfs, respectively. Under with-Project conditions, the peak flows are 58,330, 36,684, and 18,903 cfs, respectively. For Skull Creek, the peak flows for the Wet, Average and Dry years are 172, 127 and 96 cfs, respectively and are the same under existing and with-Project conditions.

The 8-year simulation period was developed using combinations of the Wet (W), Average (A) and Dry (D) years. It was assumed that on average, the Wet and Dry years occur 25 percent of the time and the Average year occurs 50 percent of the time. Therefore in any 4-year period, the Wet and Dry years each occur once and Average year occurs twice. The following time series was assumed: A-W-D-A-A-W-D-A. To determine if the sequences of floods effected the model results, a second sequence of A-D-W-A-A-D-W-A was run. To reduce the simulation time, the hydrograph period for the 7-year period was truncated to include only the high-flow period (Figure 3.3-1).

4. SUMMARY

This appendix (Appendix B) provides details of the development of the 2-D Bed Evolution Model (BEM) for FA-128 (Slough 8A). Appendix A is a parallel description of the 1-D BEM for the Middle and Lower Susitna River segments from Watana Dam to PRM 29.9. These two appendices support the analyses and results of Existing and Max LF OS-1b conditions presented as Attachment 1 of this SIR for Study 6.6. The 1-D BEM was developed to address reach-scale issues and to provide boundary condition information to the 2-D BEMs. FA-128 (Slough 8A) is the first of the focus areas to have 2-D hydraulic and sediment-transport models. The proof of concept results of the 2-D hydraulic model were presented in Tetra Tech (2014a).

The 2-D BEM provided hydraulic results comparable to the 2-D hydraulic model of FA-128 (Slough 8A) within the limitations of the coarser model network required for sediment-transport analyses. Although specific sediment-transport calibration data are not available, the model results

shows patterns of deposition and erosion that are consistent with observed changes over the past 30 years. These patterns include areas of channel widening, bar and island growth, and continued accretion of the Skull Creek fan.

Based on the results of this initial model, SRH-2D is well-suited to evaluate potential Project effects for the near term and over the license period. This includes providing future conditions information that will be applied in the detailed hydraulic model supporting habitat analysis.

5. LITERATURE CITED

Aquaveo, 2013. SMS Surface-water Modeling System, Version 11.1, User's Manual.

Barnes, H.H., 1967. Roughness characteristics of natural channels. U.S. Geological Survey Water-Supply Paper 1849.

Chow, V.T. 1959. Open Channel Hydraulics. McGraw-Hill, Inc.

Engelund, F. and Hansen, E., 1967. A Monograph on Sediment Transport Alluvial Streams. Copenhagen, Teknik Vorlag.

Greimann, B., Yong Lai, Y., and Huang, J., 2008. Two-dimensional total sediment load model equations. J. Hyd. Eng. 134:8

Hicks, D.M. and Mason, P.D., 1991. Roughness characteristics of New Zealand rivers. Water Resources Survey, DSIR Marine and Freshwater, Wellington, New Zealand.

Jarrett, R. D. 1984. Hydraulics of High-Gradient Streams. Journal of Hydraulic Engineering. ASCE, Vol. 110 (11), pp. 1519-1539.

Julien P.Y., 1995. Erosion and sedimentation. Cambridge University Press, 280 p.

Pasternack, G.B. 2011. 2-D Modeling and Ecohydraulics Analysis. Published by the University of California at Davis, Davis, California.

Parker, G., 1990. Surface-based bed-load transport relation for Gravel Rivers. J. Hydraul. Res., 28(4), pp. 417-436.

R2 Resource Consultants, Inc. (R2). 2014. Fish and Aquatics Instream Flow Study. Initial Study Report (8.5) prepared for Alaska Energy Authority Susitna-Watana Hydroelectric Project. FERC No. 14241.

Sontec/YSI. 2013. RiverSurveyor S5/M9 System Manual. www.sontec.com

Tetra Tech. 2014a. Updated Fluvial Geomorphology Approach. Technical Memorandum including Attachment A: FA-128 (Slough 8A) Hydraulic Modeling for Proof of Concept. Susitna-Watana Hydroelectric Project. Prepared for the Alaska Energy Authority. Anchorage, Alaska.

Tetra Tech. 2014b. Winter Sampling of Main Channel Bed Material. Technical Memorandum. Susitna-Watana Hydroelectric Project. Prepared for the Alaska Energy Authority. Anchorage, Alaska.

Wilcock, P.R., and Crowe, J.C., 2003. Surface-based transport model for mixed-size sediment. Journal of Hydraulic Engineering 129, pp. 120-128.

6. TABLES

Table 2.3-1. Summary of ADCP flow measurements at FA-128 (Table modified from ISR8.5).

Date/Time	Transect	Flow (cfs)					Total Flow
		Far left	Left	Middle	Right	Far right	cfs
7/2/13 13:14	T1		7,520		17,197		24,717
7/2/13 12:46	T2	6,204	236	766	17,710		24,916
7/2/13 12:12	T3		379	5,843	18,413		24,635
7/2/13 11:26	T4	9.10	374	2,629	12,818	8,745	24,575
7/2/13 10:58	T5			24,538			24,538
7/2/13 12:24	T6			231			24,651
7/2/13 15:36	T7			2.95			24,905
						Average	24,705
9/10/13 14:03	T1		8,547		17,551		26,098
9/10/13 13:40	T2	6,960	250	884	18,019		26,113
9/10/13 13:13	T3		473	6,331	19,328		26,132
9/10/13 12:20	T4	No Measurement	473	2,907	13,659	9,127	26,167
9/10/13 11:54	T5			26,184			26,184
9/10/13 13:26	T6			250			
9/10/13 15:10	T7			3.68			
						Average	26,124

Table 2.3-2. Summary of water-surface elevation measurements and model validation at FA-128.

Date	Source	Discharge (cfs)	Number of WSE Measurements	Average Difference (ft) (predicted – measured)
2-Jul-2013[A]	Geovera, LLC	24,705	32	-0.1
24-Jul-2013	Geovera, LLC	20,132	129	0.06
26-Jul-2013	Geovera, LLC	20,497	199	0.3
10-Sep-2013[A]	Geovera, LLC	26,124	32	-0.3

[A]ADCP measurements collected.

Table 2.3-3. Comparison of the predicted and measured flows collected on September, 10, 2013, when the discharge in the river was approximately 26,124 cfs.

Transect	Measured		Hydraulic Model			
	Flow (cfs)	% of Total Flow	Predicted (cfs)	% of Total Flow	Difference. (cfs)	% Difference
T1A	8,547	33	8,647	33	100	1.2
T1B	17,551	67	17,473	67	-78	-0.4
T2A	6,960	27	6,949	27	-11	-0.2
T2B	250[A]	1.0	285	1.1	35	14.1
T2C	884	3.4	943	3.6	59	6.6
T2D	18,019	69	17,943	69	-76	-0.4
T3A	473	1.8	518	2.0	45	9.6
T3B	6,331	24	6,431	25	100	1.6
T3C	19,328	74	19,175	73	-153	-0.8
T4A	No Meas.					
T4B	473	1.8	503	1.9	30	6.3
T4C	2,907	11	3,290	13	383	13.2
T4D	13,659	52	13,114	50	-545	-4.0
T4E	9,127	35	9,202	35	75	0.8
T5	26,184	100	26,184	100	0	0.0
T6	250	1.0	285	1.1	35	14.1
T7	3.7	0.01	4.8	0.02	1.1	30.6

Note: [A] No measurement but should be the same as T6.

Table 2.3-4. Comparison of the predicted and measured flows collected on July 2, 2013, when the discharge in the river was approximately 24,705 cfs.

Transect	Measured		Hydraulic Model			
	Flow (cfs)	Percent of Total Flow	Predicted (cfs)	Percent of Total Flow	Difference. (cfs)	Percent Difference
T1A	7,520	30	7,873	32	353	4.7
T1B	17,197	70	16,831	68	-365	-2.1
T2A	6,204	25	6,409	26	205	3.3
T2B	236	1.0	239	1.0	-11	-4.3
T2C	766	3.1	814	3.3	48	6.2
T2D	17,710	72	17,243	70	-467	-2.6
T3A	379	1.5	441	1.8	62	16.3
T3B	5,843	24	5,968	24	125	2.1
T3C	18,413	75	18,297	74	-117	-0.6
T4A	9.1	0.04	26	0.11	17	188.0
T4B	374	1.5	414	1.7	41	10.9
T4C	2,629	10.6	3,012	12	383	14.6
T4D	12,818	52	12,543	51	-275	-2.1
T4E	8,745	35	8,710	35	-35	-0.4
T5	24,705	100	24,705	100	0.0	0.0
T6	231	0.9	239	1.0	8.2	3.5
T7	3.0	0.01	5.4	0.02	2.5	83.7

7. FIGURES

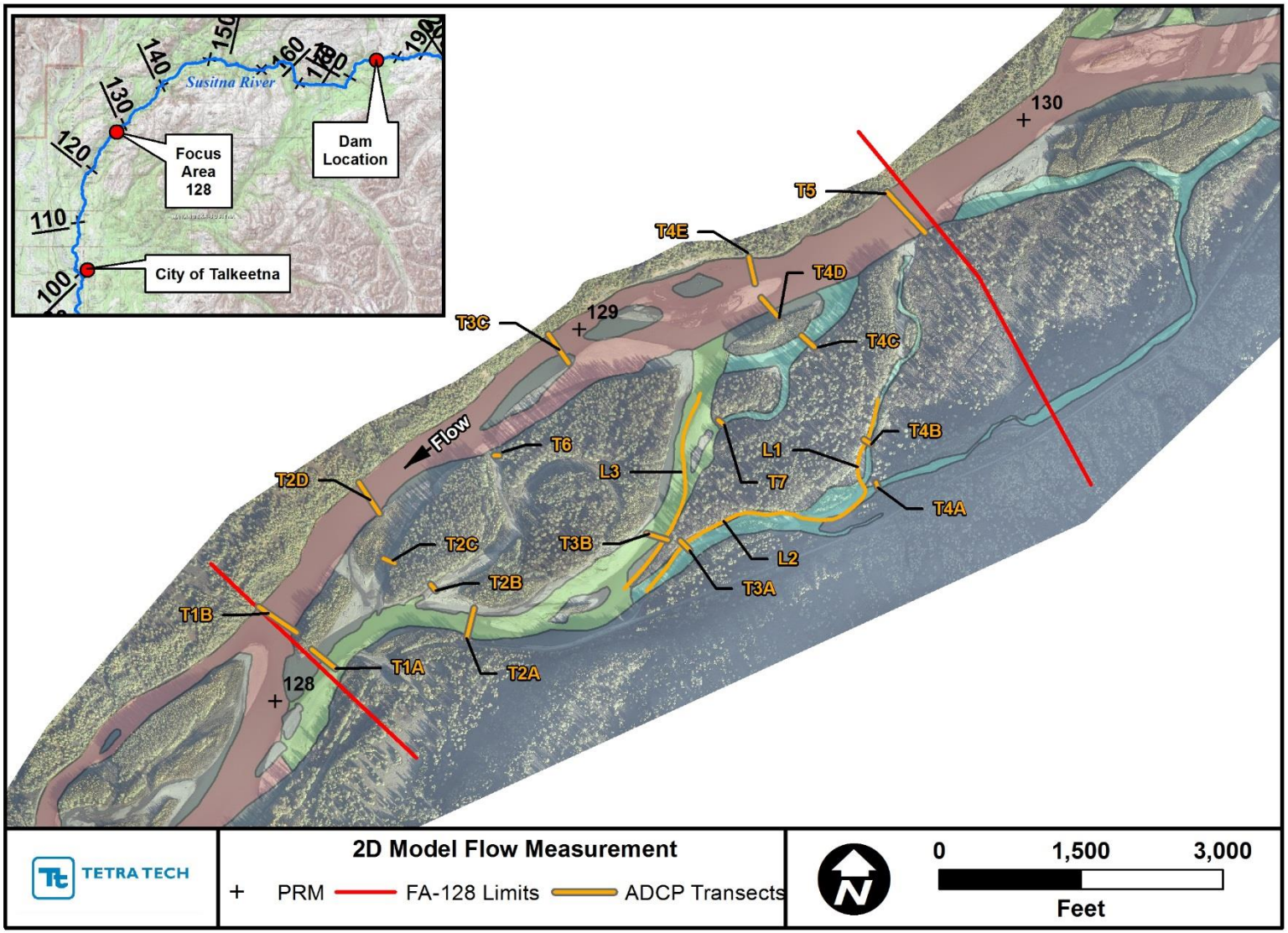

Figure 1-1. Site location map and location of ADCP transects.

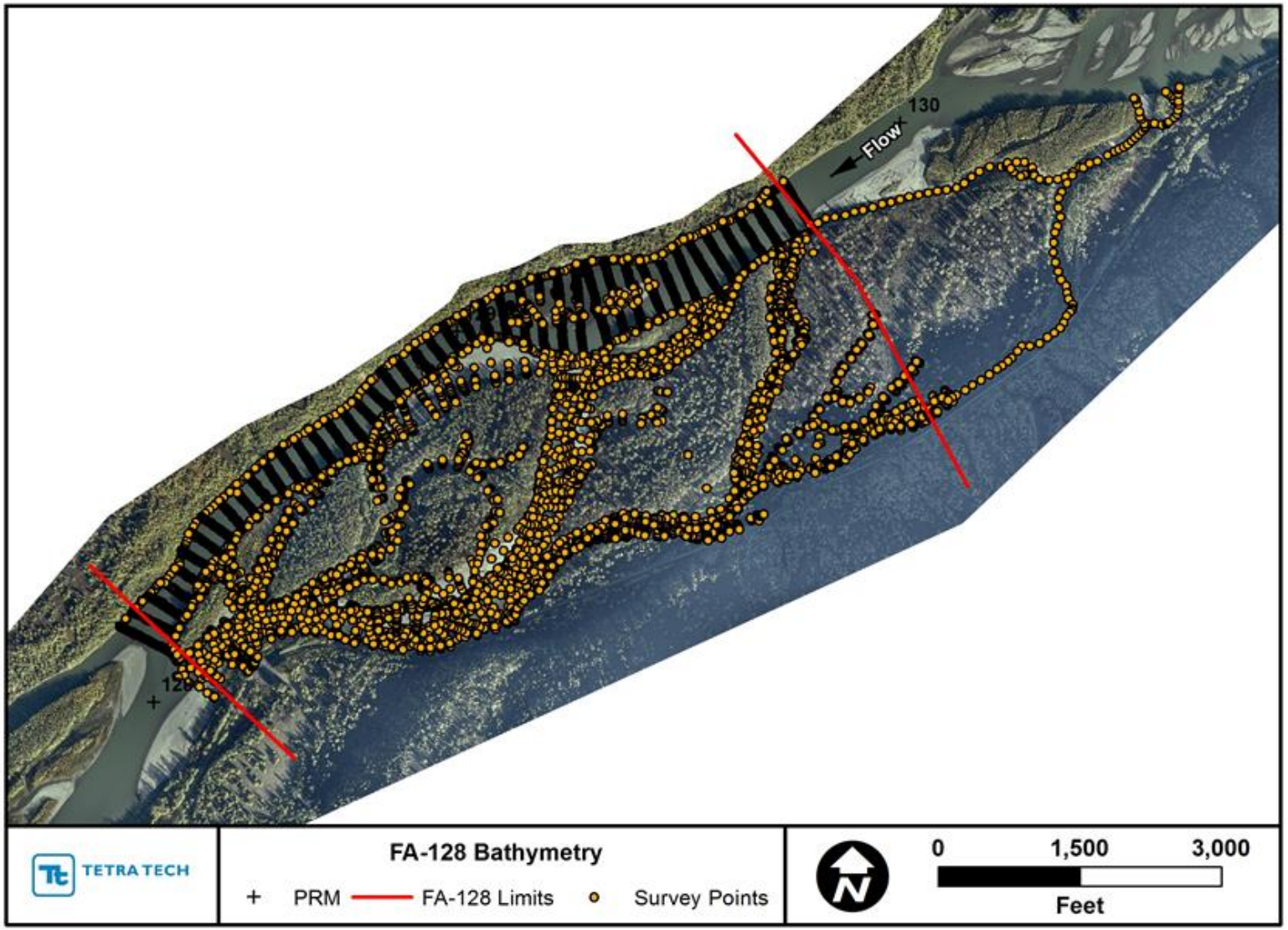

Figure 2.2-1. Bathymetric and topographic survey data collected at FA-128 (Skull Creek).

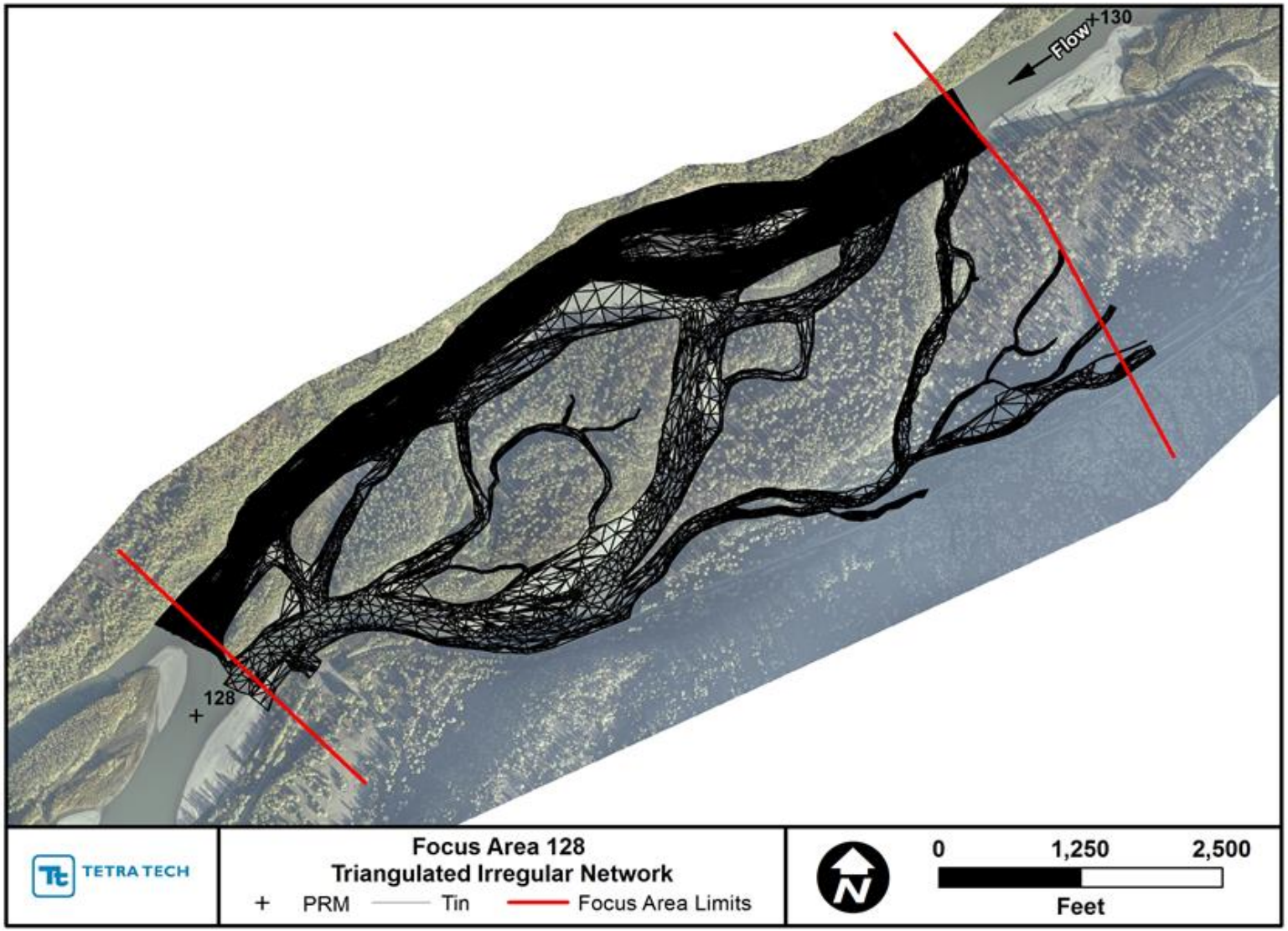

Figure 2.2-2. Triangular Irregular Network (TIN) developed for the in-channel areas using the topographic and bathymetric data shown in Figure 2.2-3. Note: the in-channel TIN was merged with the overbank TIN developed from the 2012 LiDAR data (not shown).

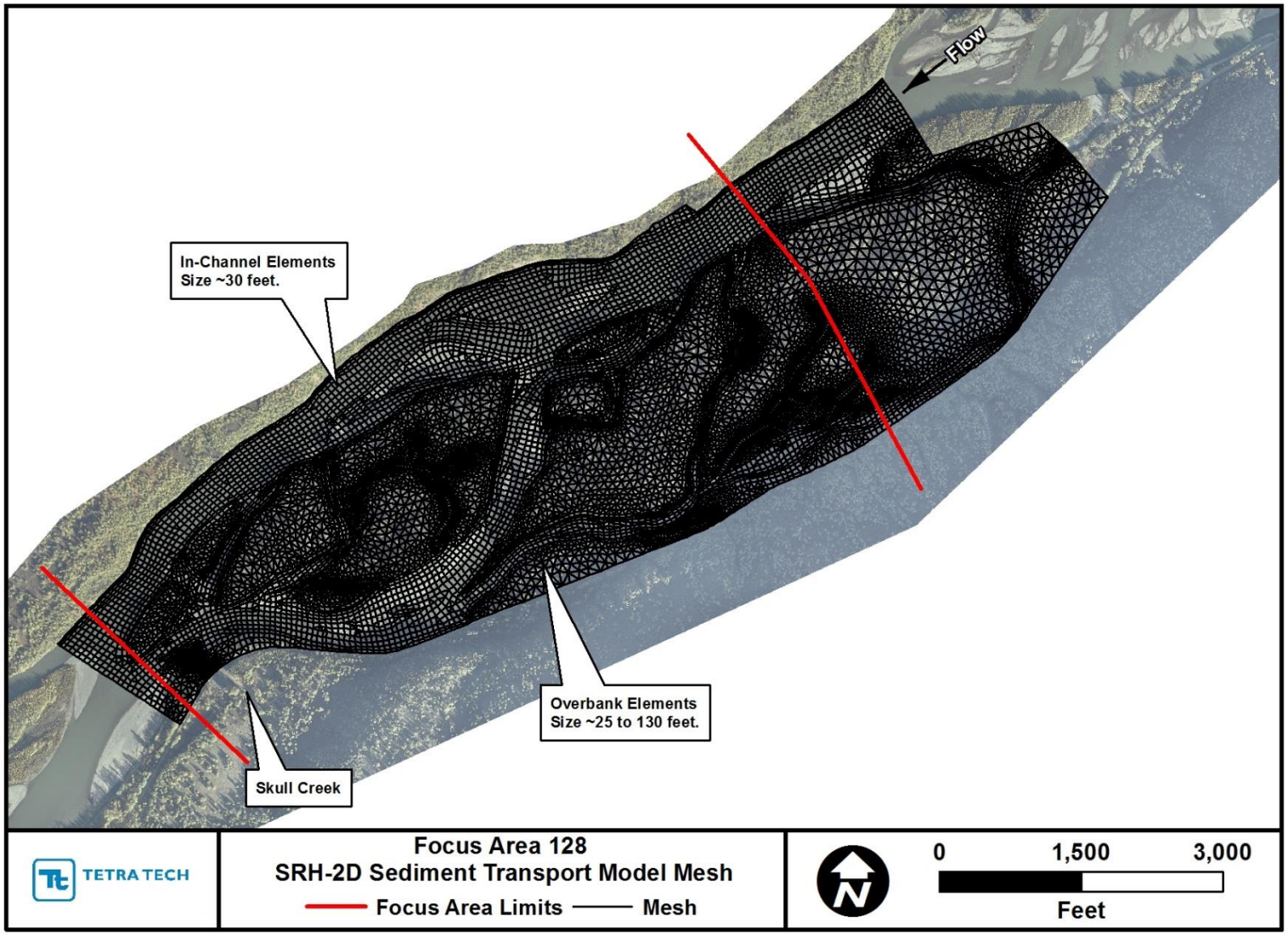

Figure 2.2-3. FA-128 SRH-2D sediment-transport model mesh.

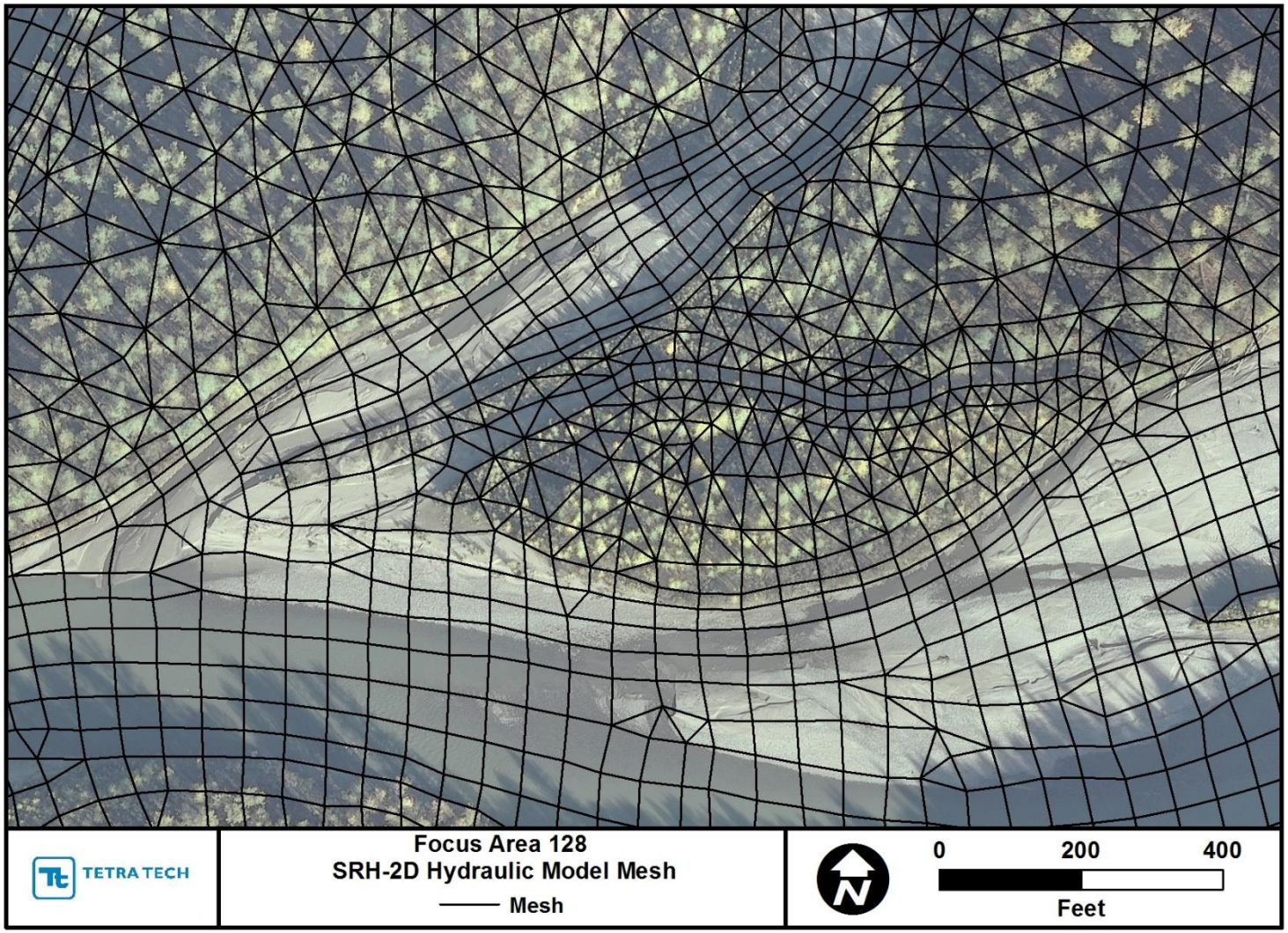

Figure 2.2-4. Close-up of the FA-128 SRH-2D sediment-transport model mesh.

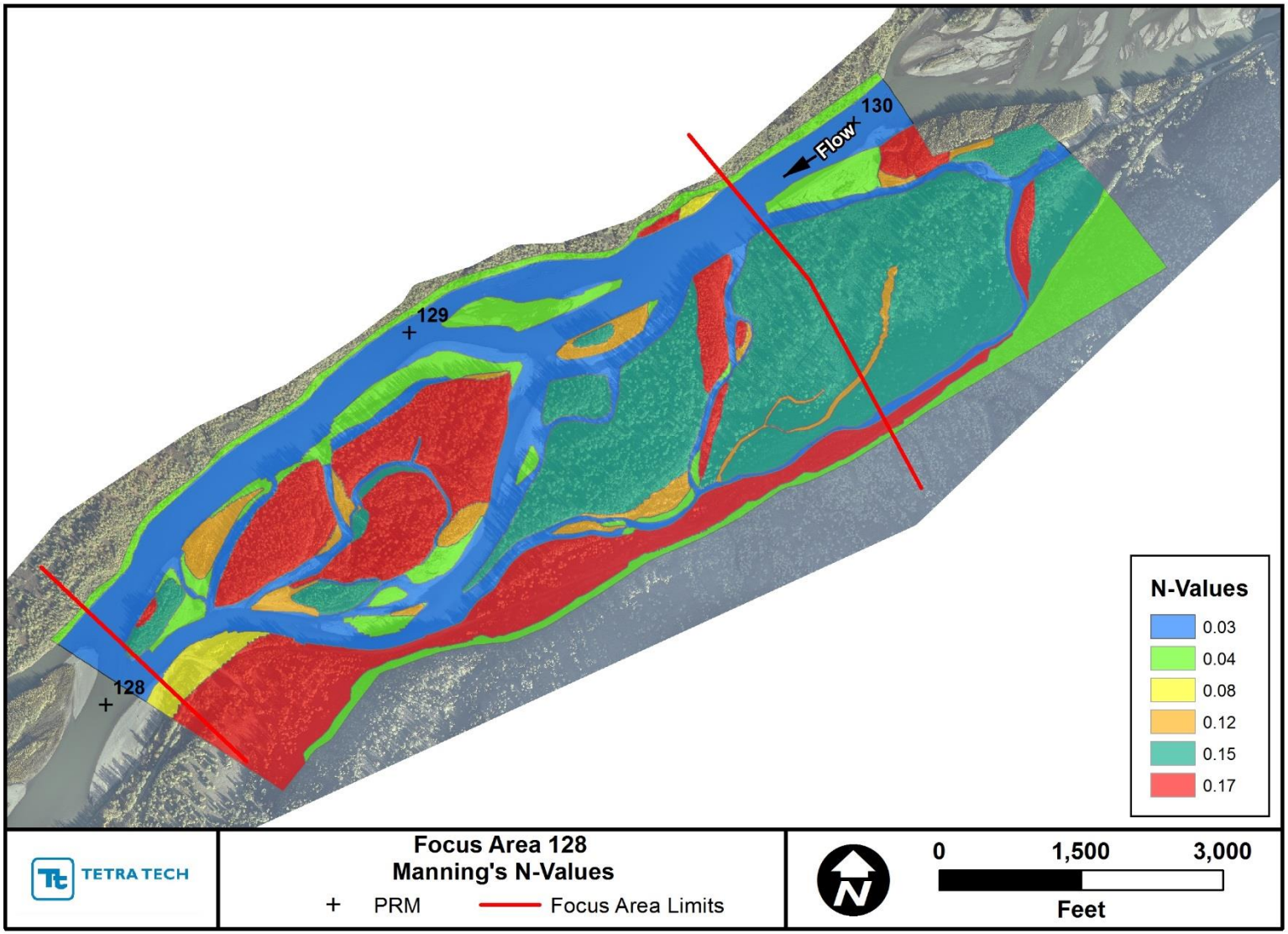

Figure 2.2-5. Manning's n-values applied to the SRH-2D models.

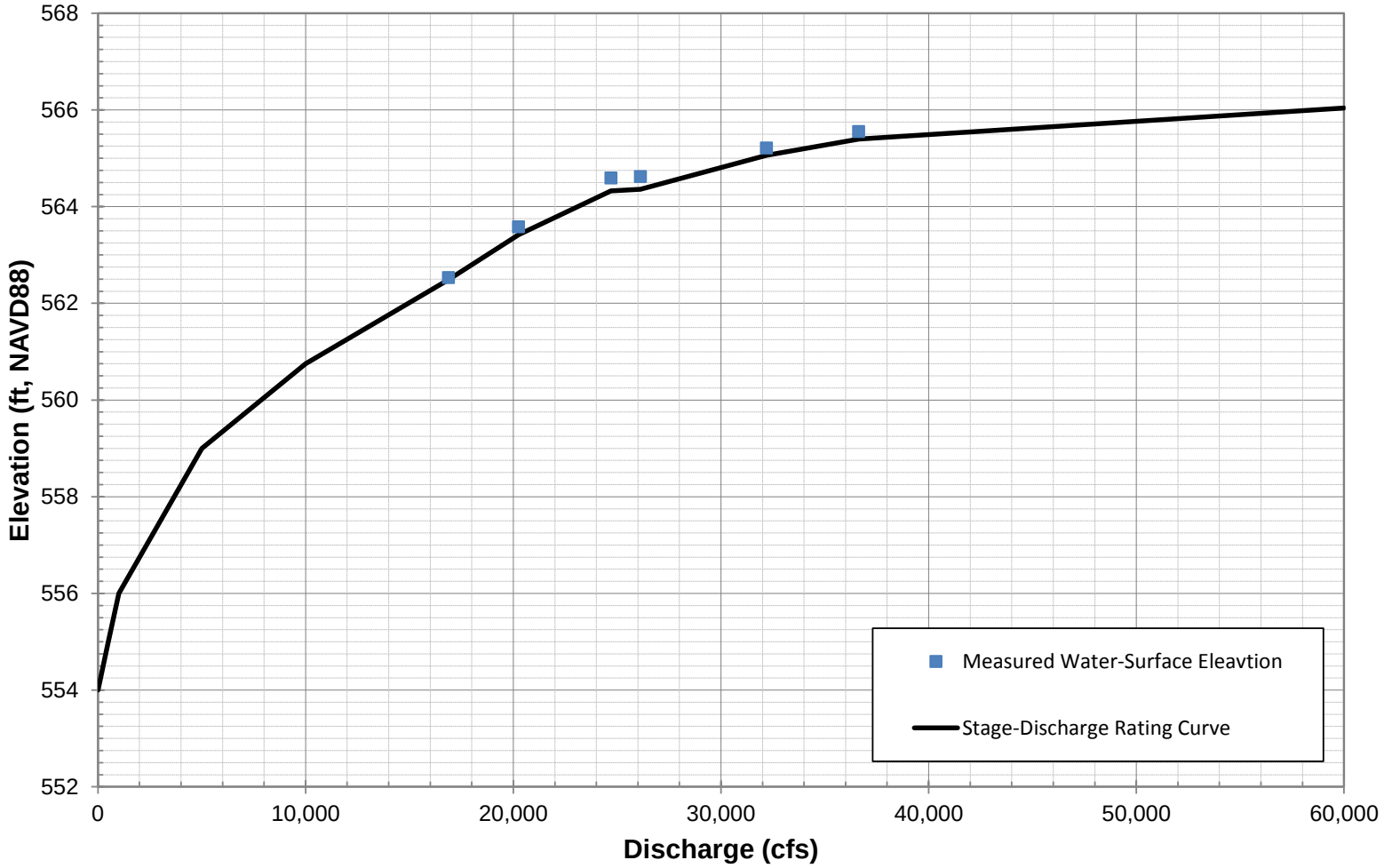

Figure 2.2-6. Stage-discharge rating curve applied to the downstream boundary of the 2-D model.

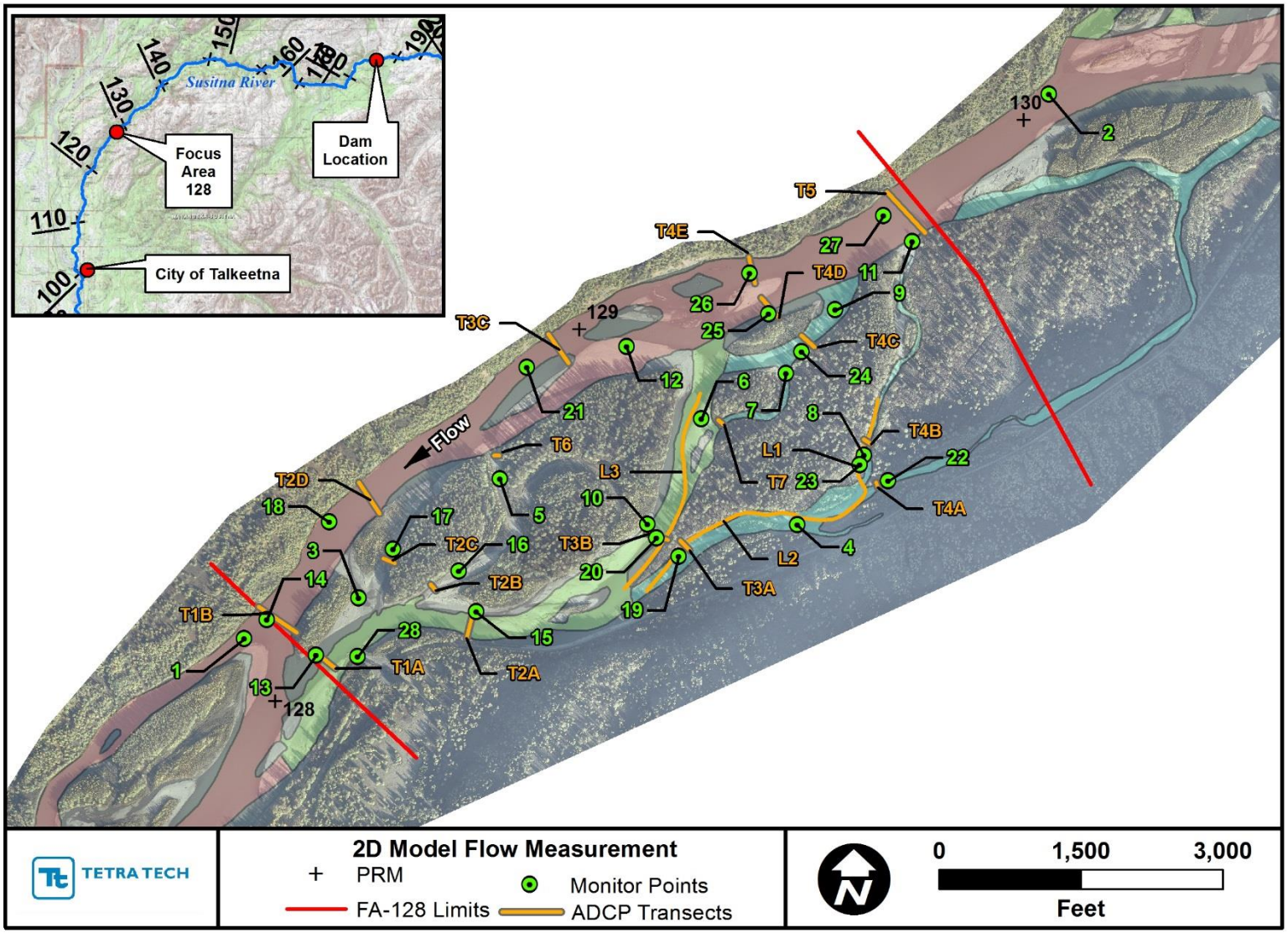

Figure 2.2-7. Location of the ADCP transects and selected monitor points used to evaluate the model output.

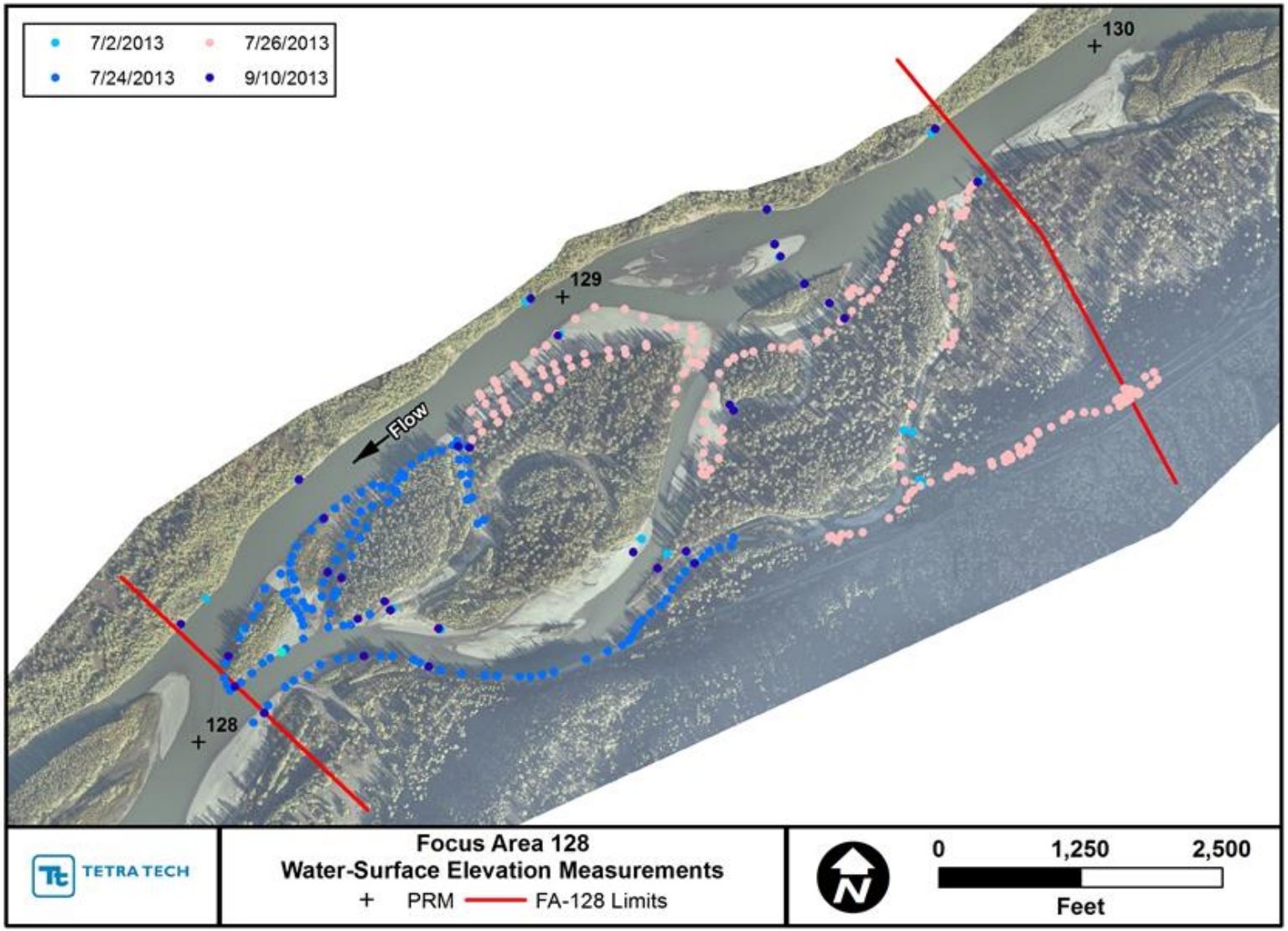

Figure 2.2-8. Location of the measured water-surface elevations (WSE's).

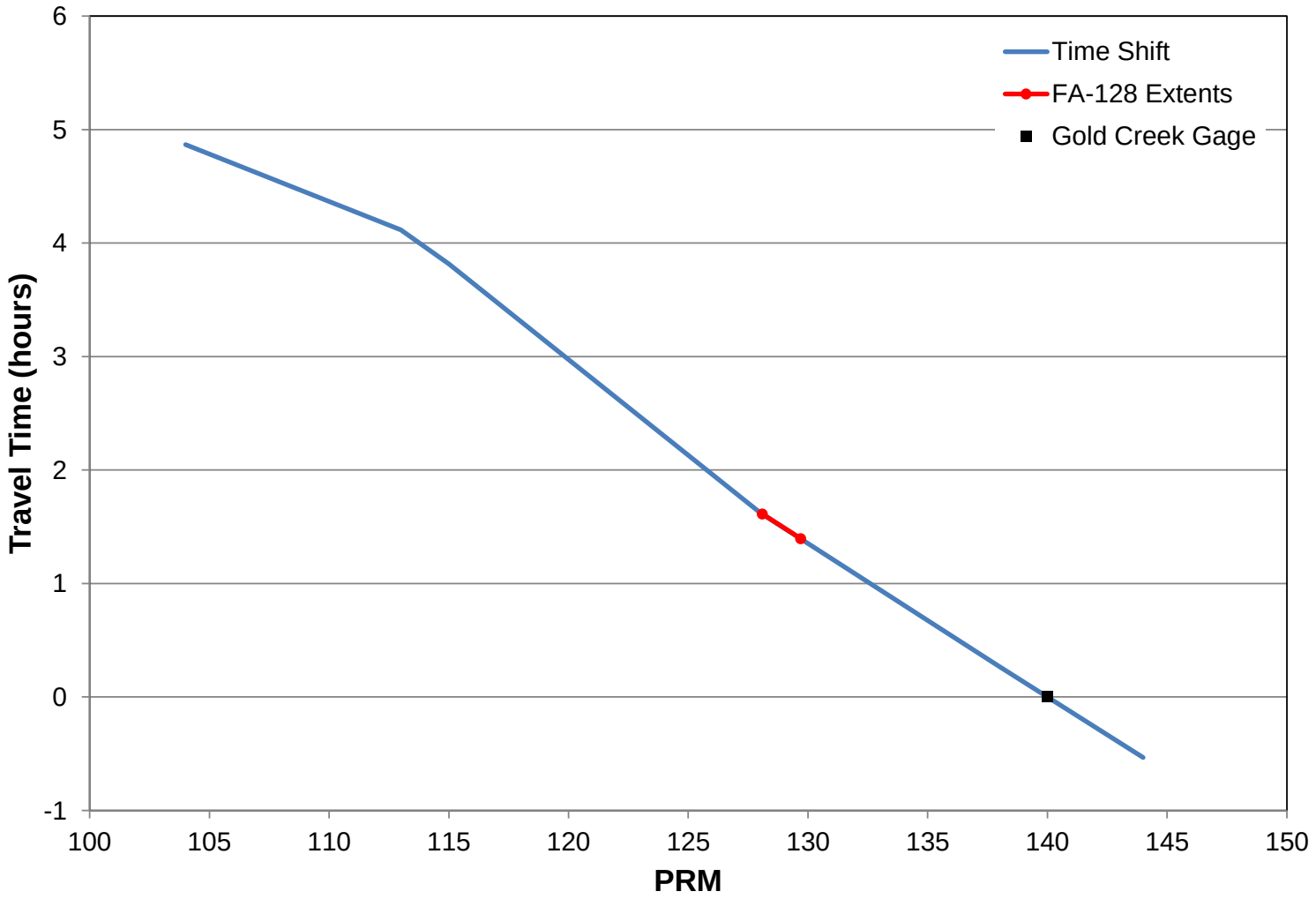

Figure 2.3-1. Flow travel time along the middle reach from Gold Creek gage. The travel times at each Focus Area are reported in ISR 8.5.

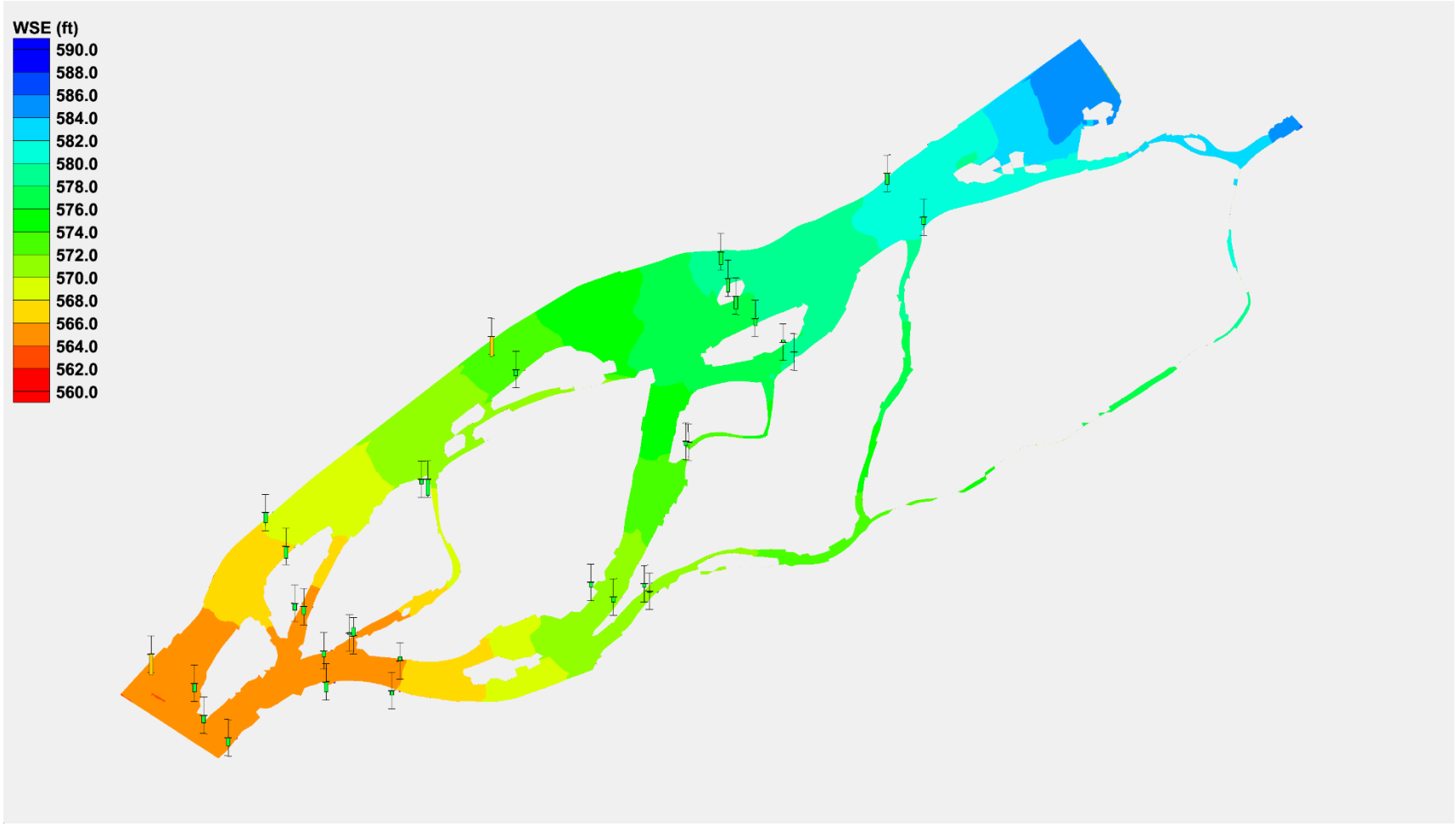

Figure 2.3-2. Screen capture from SMS showing differences between the measured and predicted water-surface elevations from the hydraulic model at 26,124 cfs (September 10, 2013).

The bars indicate the relative differences in water-surface elevations in the direction of the error. For example, if the color is in the lower half, then the predicted water-surface elevation is lower than the measured values. Green bars indicate differences of less than 0.5 feet, and orange bars indicated differences between 0.5 and 1 foot.

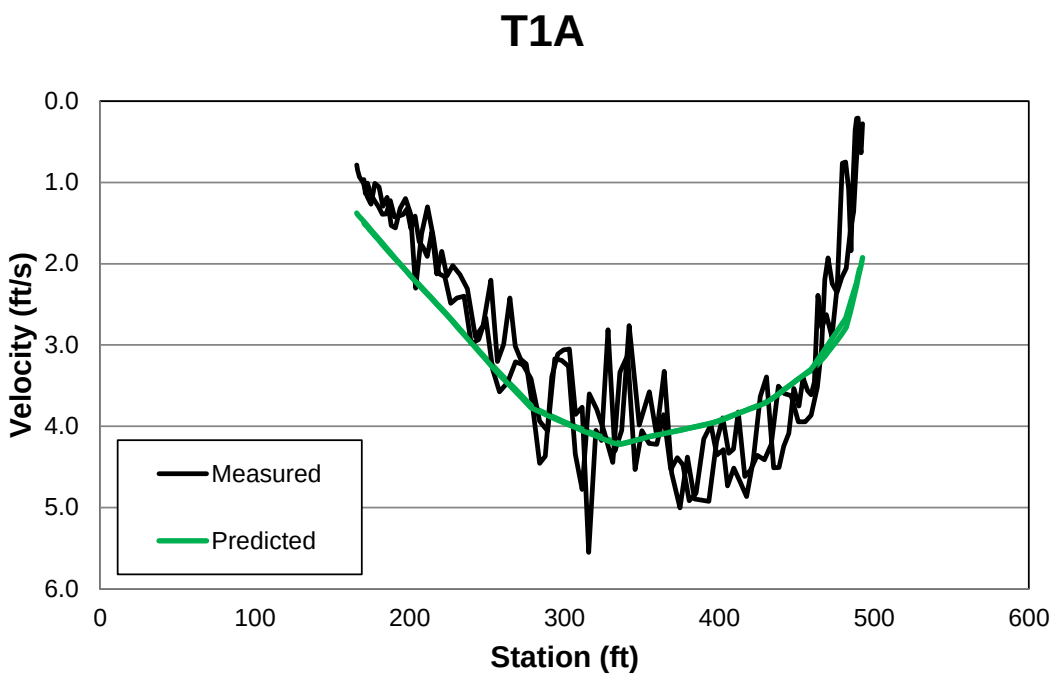

Figure 2.3-3. Comparison of measured velocities with the predicted velocities at Transect 1A (Figure 2.2-7) at 26,184 cfs (Sept.10, 2013).

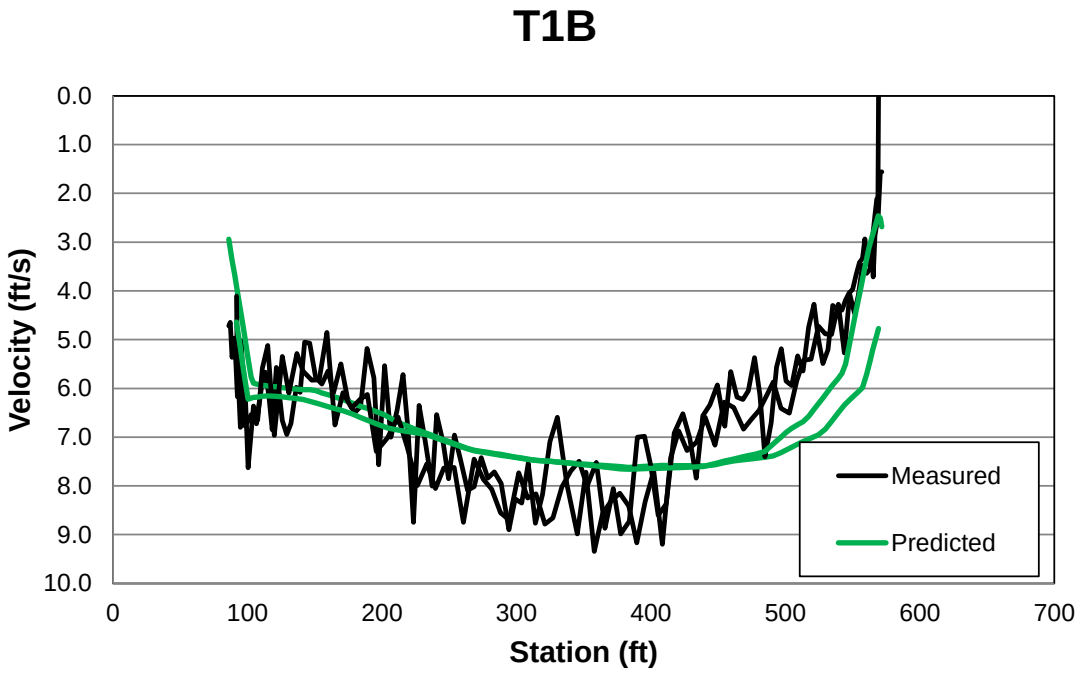

Figure 2.3-4. Comparison of measured velocities with the predicted velocities at Transect 1B (Figure 2.2-7) at 26,184 cfs (Sept. 10, 2013).

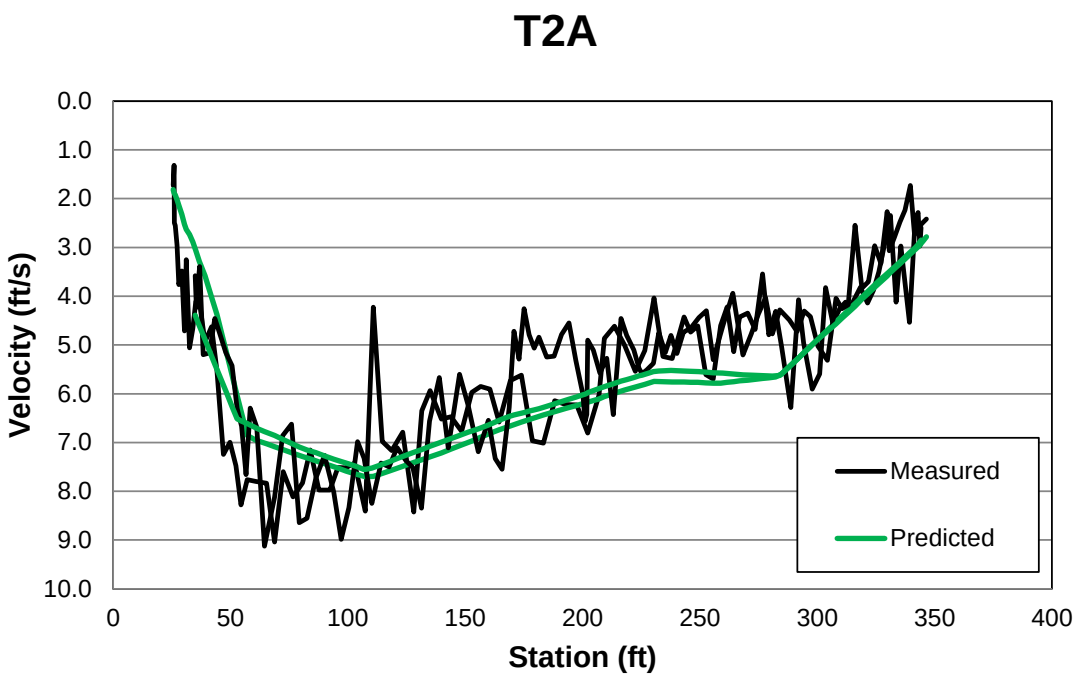

Figure 2.3-5. Comparison of measured velocities with the predicted velocities at Transect 2A (Figure 2.2-7) at 26,184 cfs (Sept. 10, 2013).

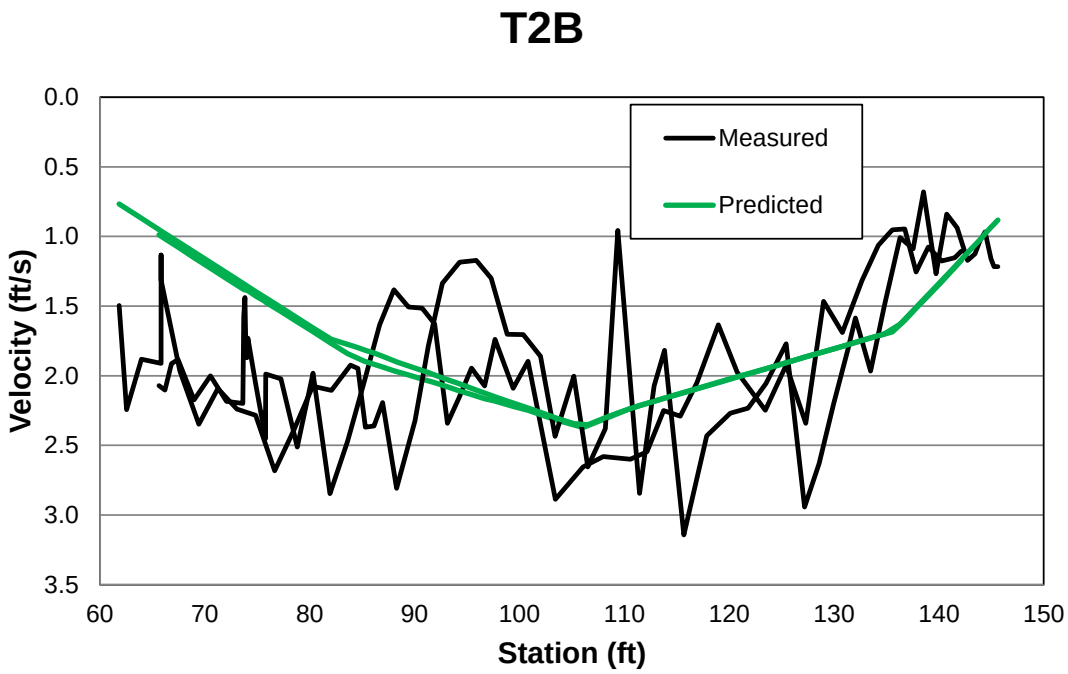

Figure 2.3-6. Comparison of measured velocities with the predicted velocities at Transect 2B (Figure 2.2-7) at 26,184 cfs (Sept. 10, 2013).

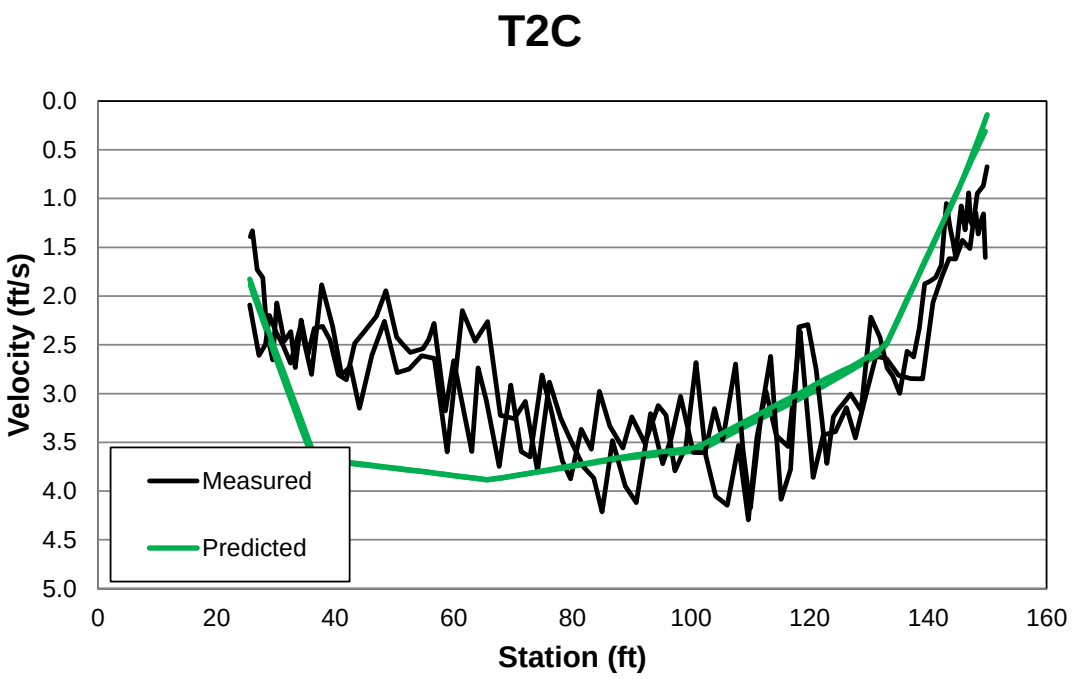

Figure 2.3-7. Comparison of measured velocities with the predicted velocities at Transect 2C (Figure 2.2-7) at 26,184 cfs (Sept. 10, 2013).

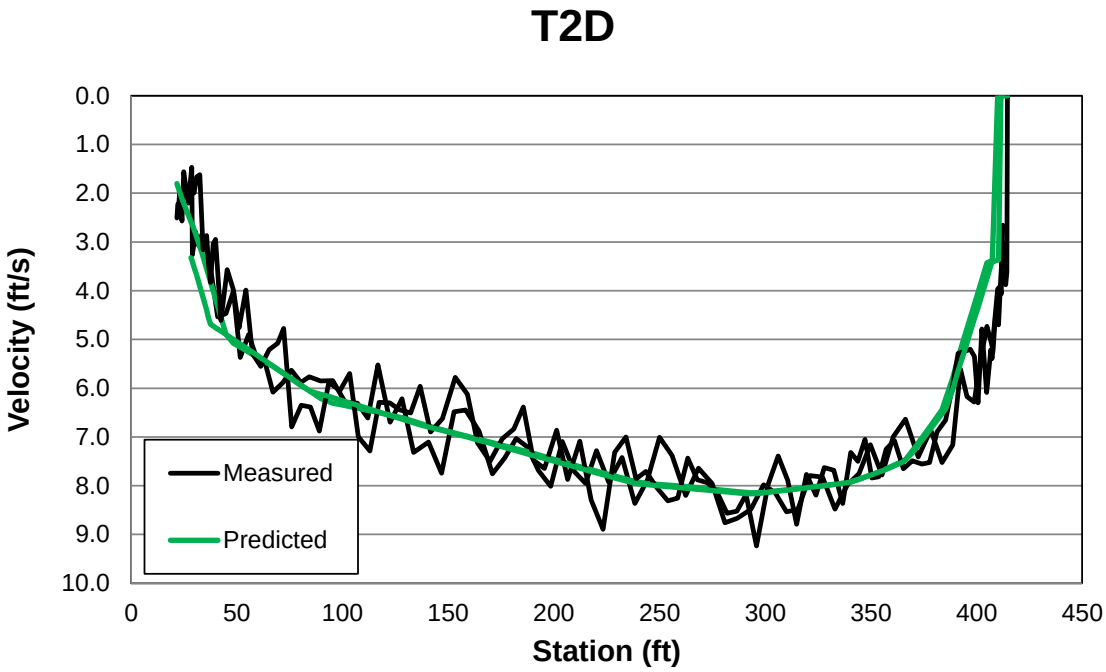

Figure 2.3-8. Comparison of measured velocities with the predicted velocities at Transect 2D (Figure 2.2-7) at 26,184 cfs (Sept. 10, 2013).

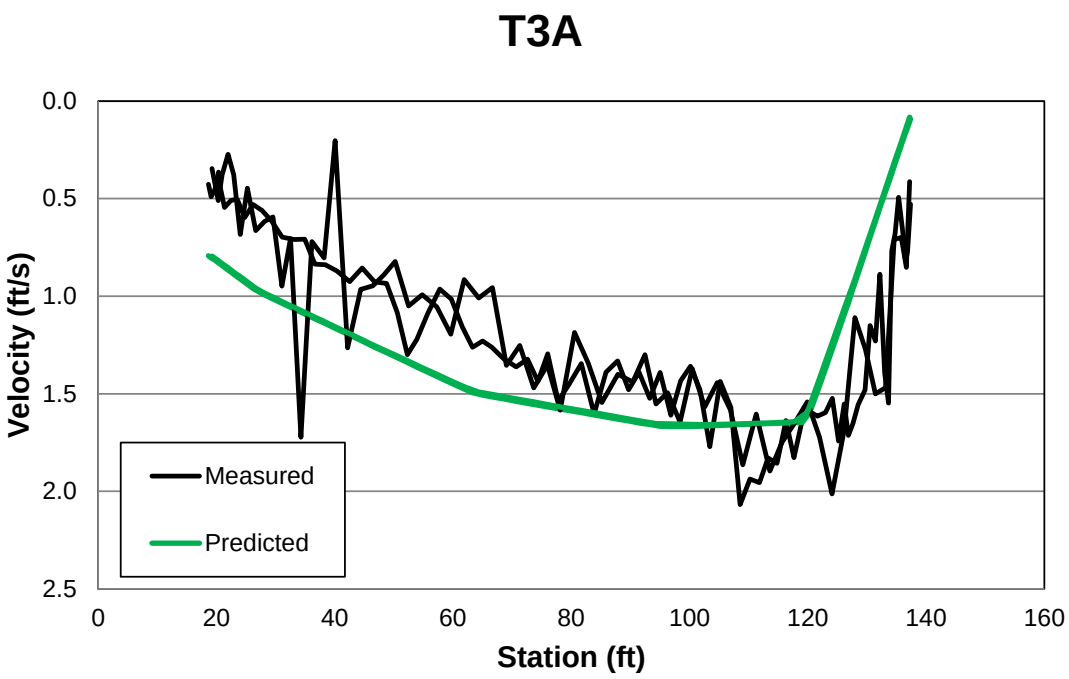

Figure 2.3-9. Comparison of measured velocities with the predicted velocities at Transect 3A (Figure 2.2-7) at 26,184 cfs (Sept. 10, 2013).

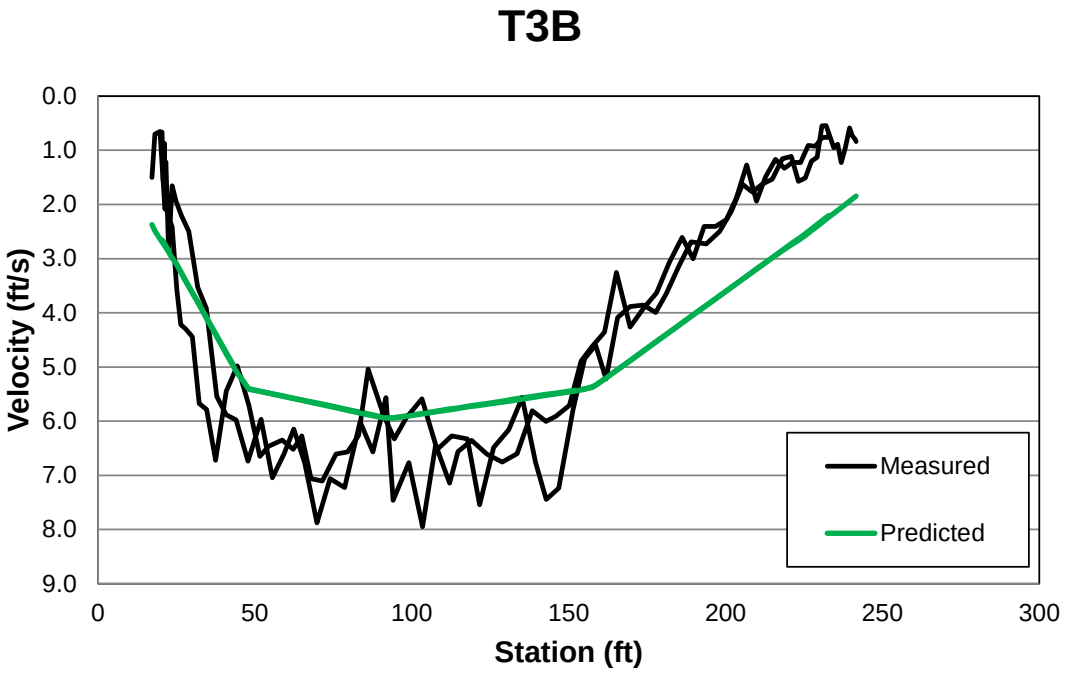

Figure 2.3-10. Comparison of measured velocities with the predicted velocities at Transect 3B (Figure 2.2-7) at 26,184 cfs (Sept. 10, 2013).

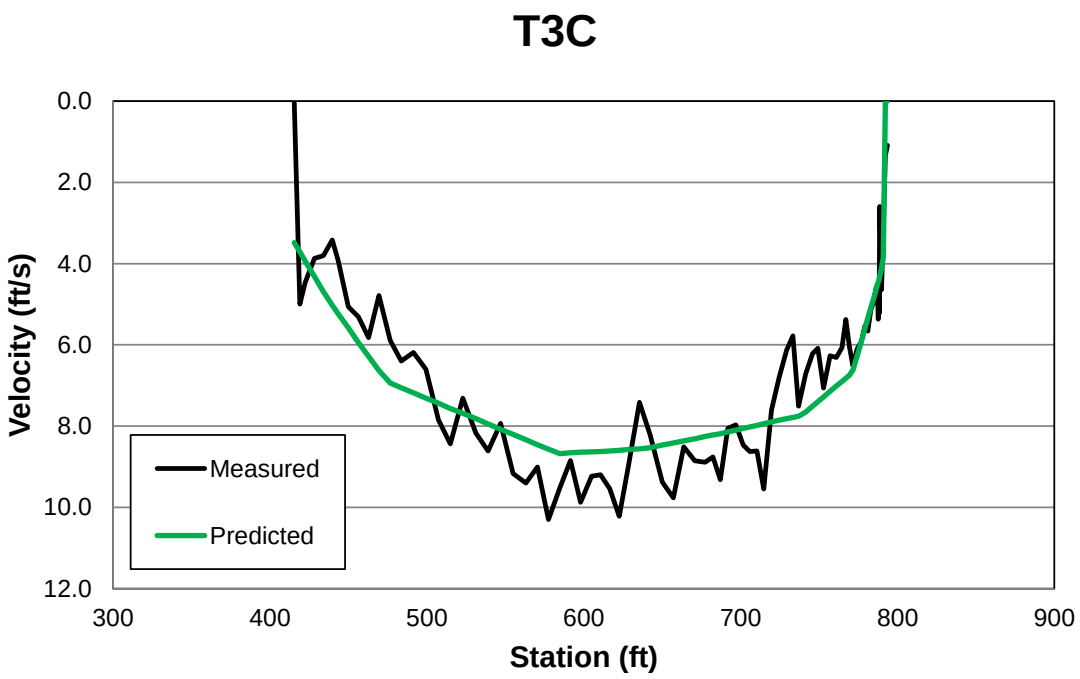

Figure 2.3-11. Comparison of measured velocities with the predicted velocities at Transect 3C (Figure 2.2-7) at 26,184 cfs (Sep 10, 2013).

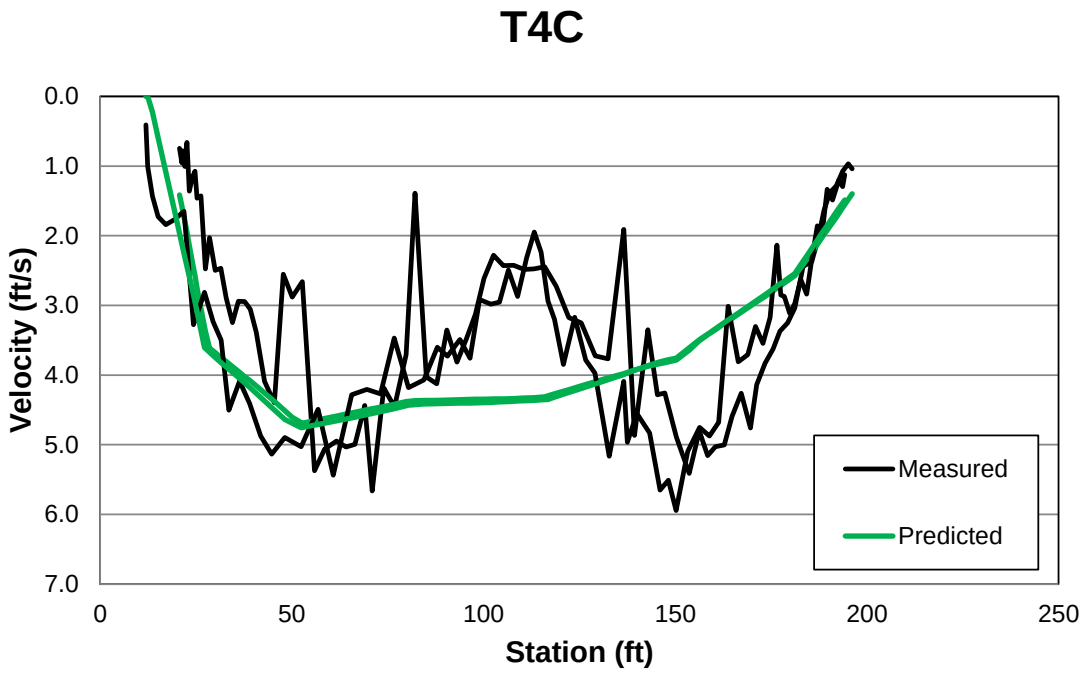

Figure 2.3-12. Comparison of measured velocities with the predicted velocities at Transect 4C (Figure 2.2-7) at 26,184 cfs (Sept. 10, 2013).

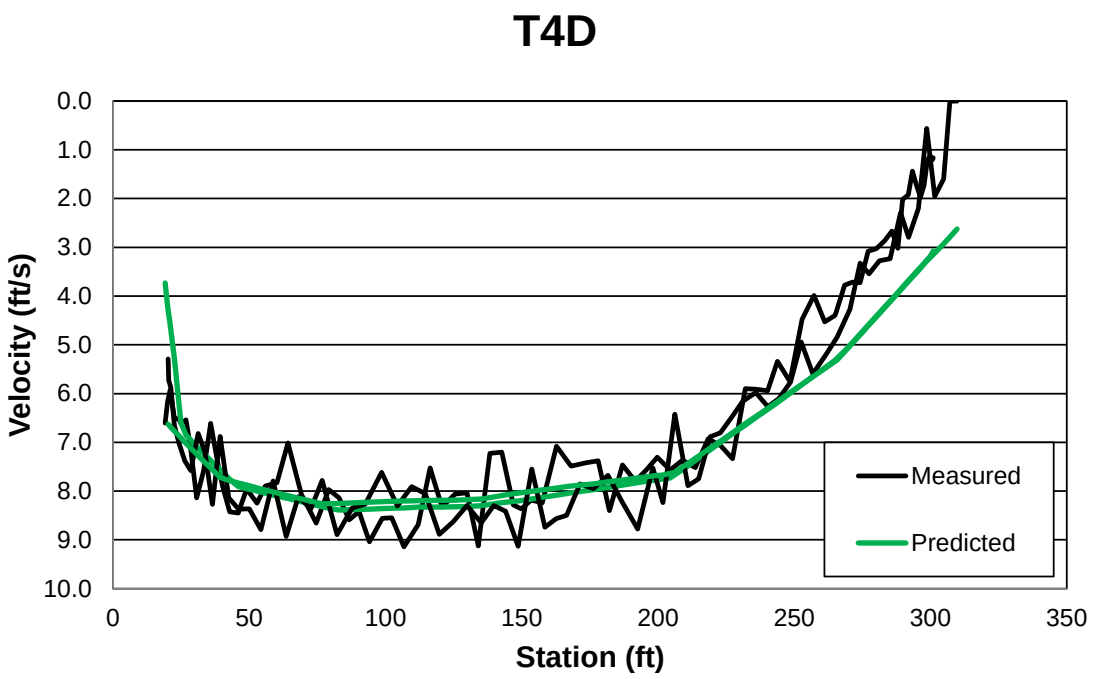

Figure 2.3-13. Comparison of measured velocities with the predicted velocities at Transect 4D (Figure 2.2-7) at 26,184 cfs (Sept. 10, 2013).

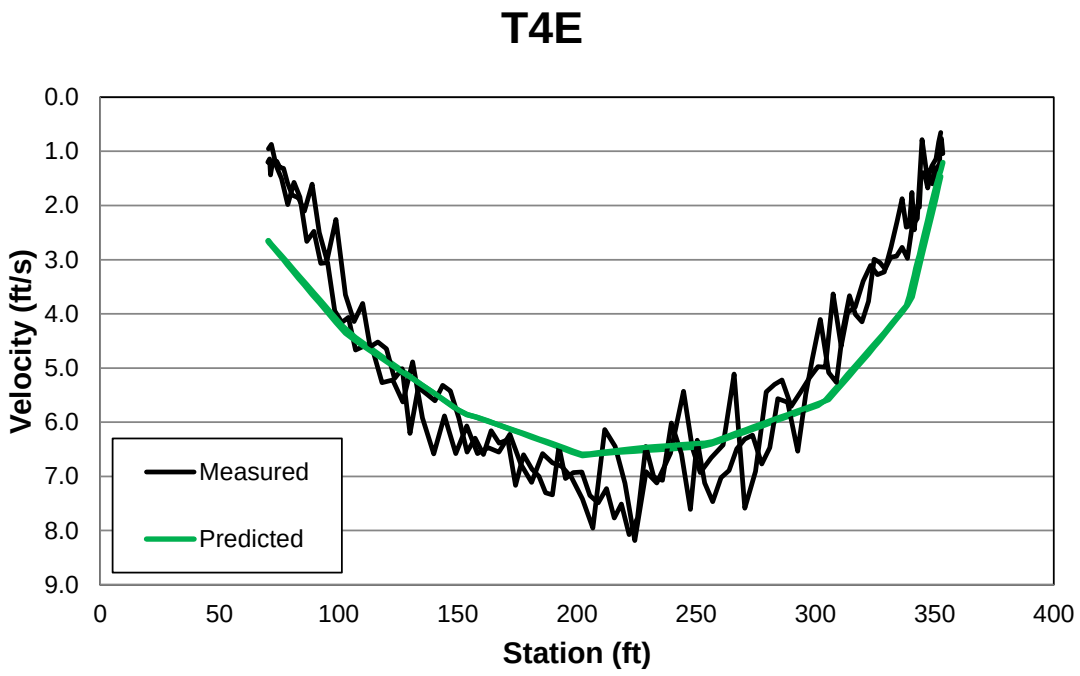

Figure 2.3-14. Comparison of measured velocities with the predicted velocities at Transect 4E (Figure 2.2-7) at 26,184 cfs (Sept. 10, 2013).

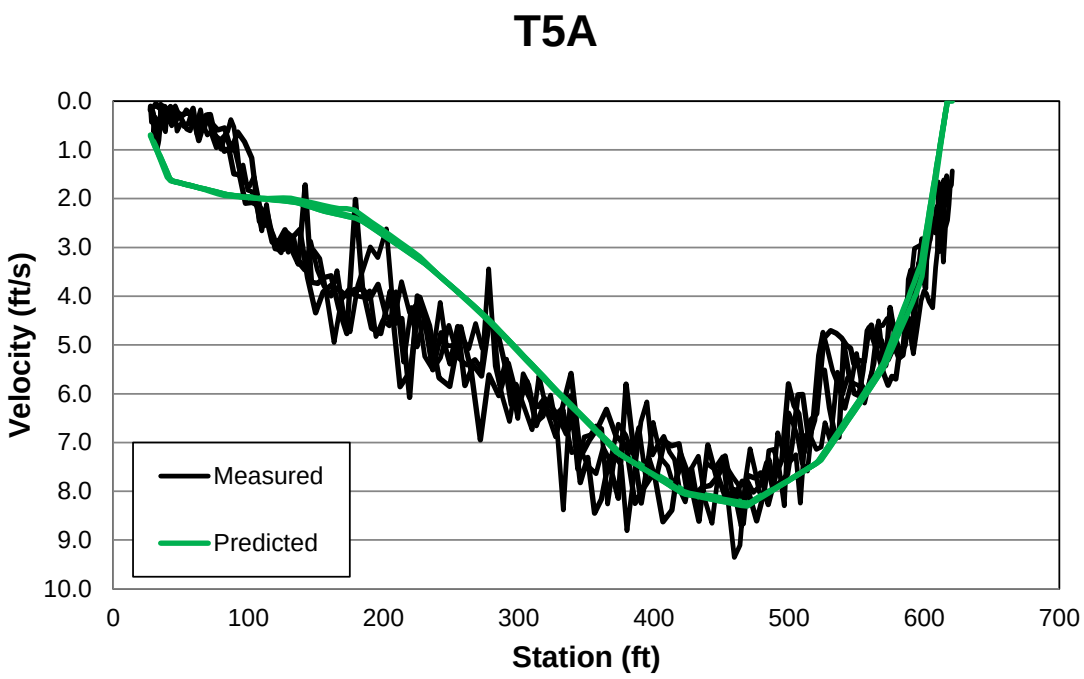

Figure 2.3-15. Comparison of measured velocities with the predicted velocities at Transect 5A (Figure 2.2-7) at 26,184 cfs (Sept. 10, 2013).

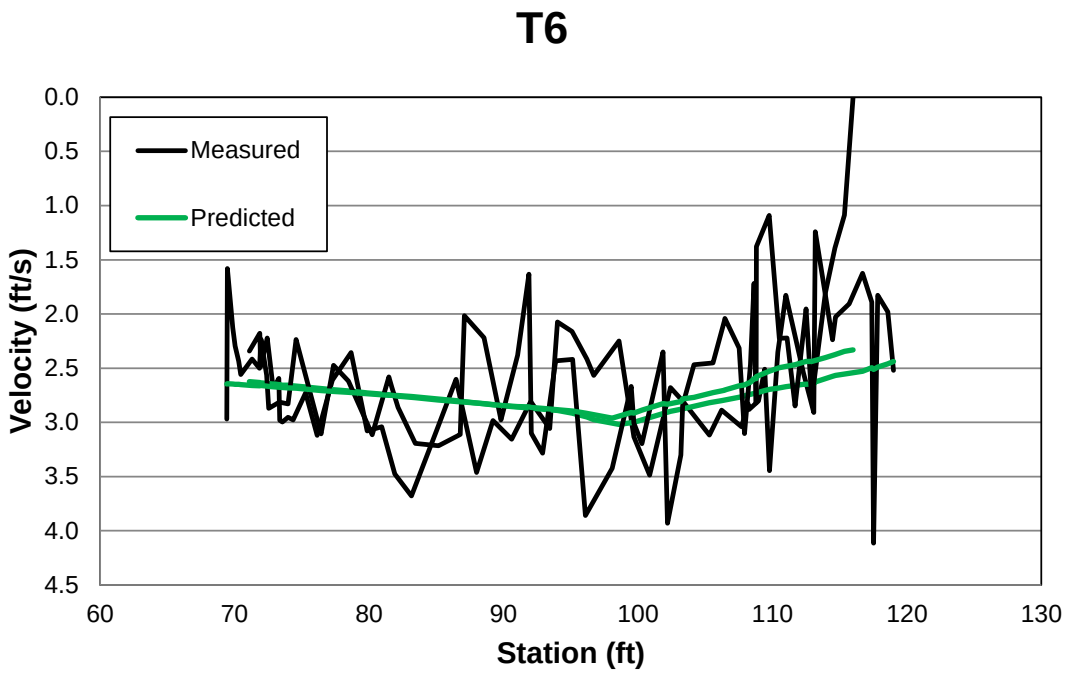

Figure 2.3-16. Comparison of measured velocities with the predicted velocities at Transect 6 (Figure 2.2-7) at 26,184 cfs (Sept. 10, 2013).

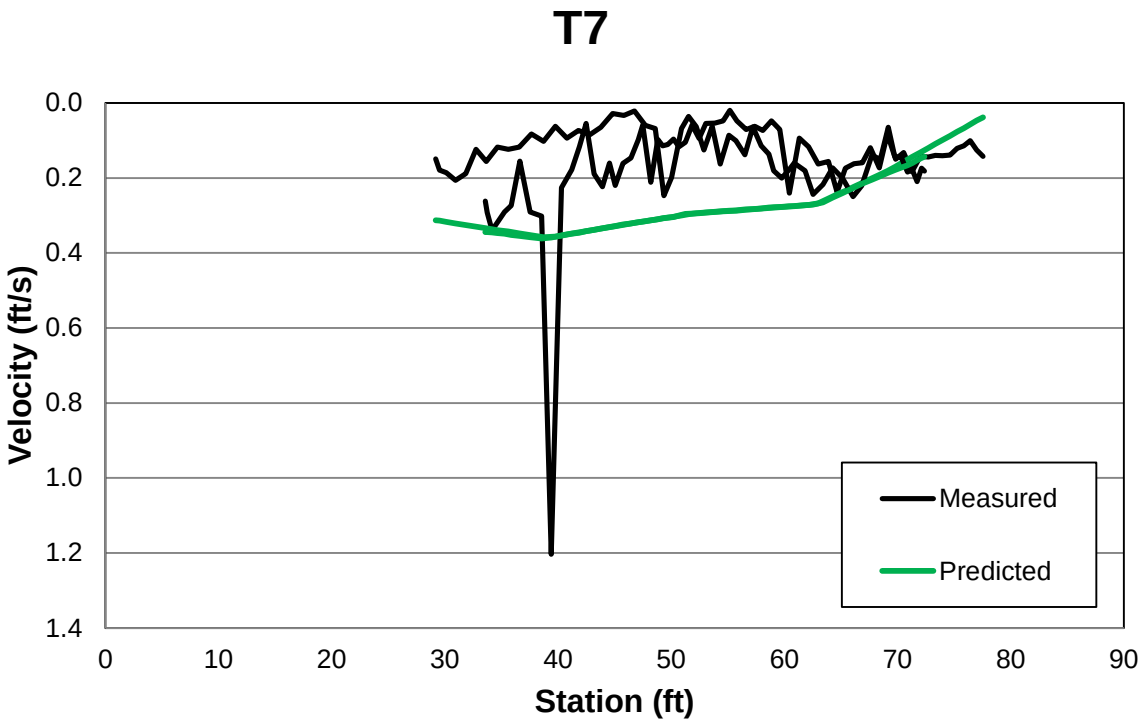

Figure 2.3-17. Comparison of measured velocities with the predicted velocities at Transect 7 (Figure 2.2-7) at 26,184 cfs (Sept. 10, 2013).

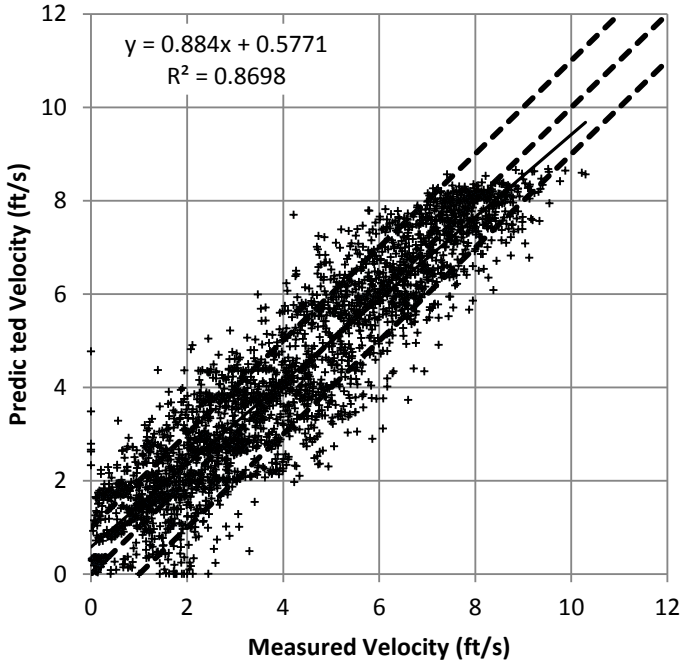

Figure 2.3-18. Scatter plot showing difference in velocity (predicted – measured) at 26,124 cfs (Sept. 10, 2013).

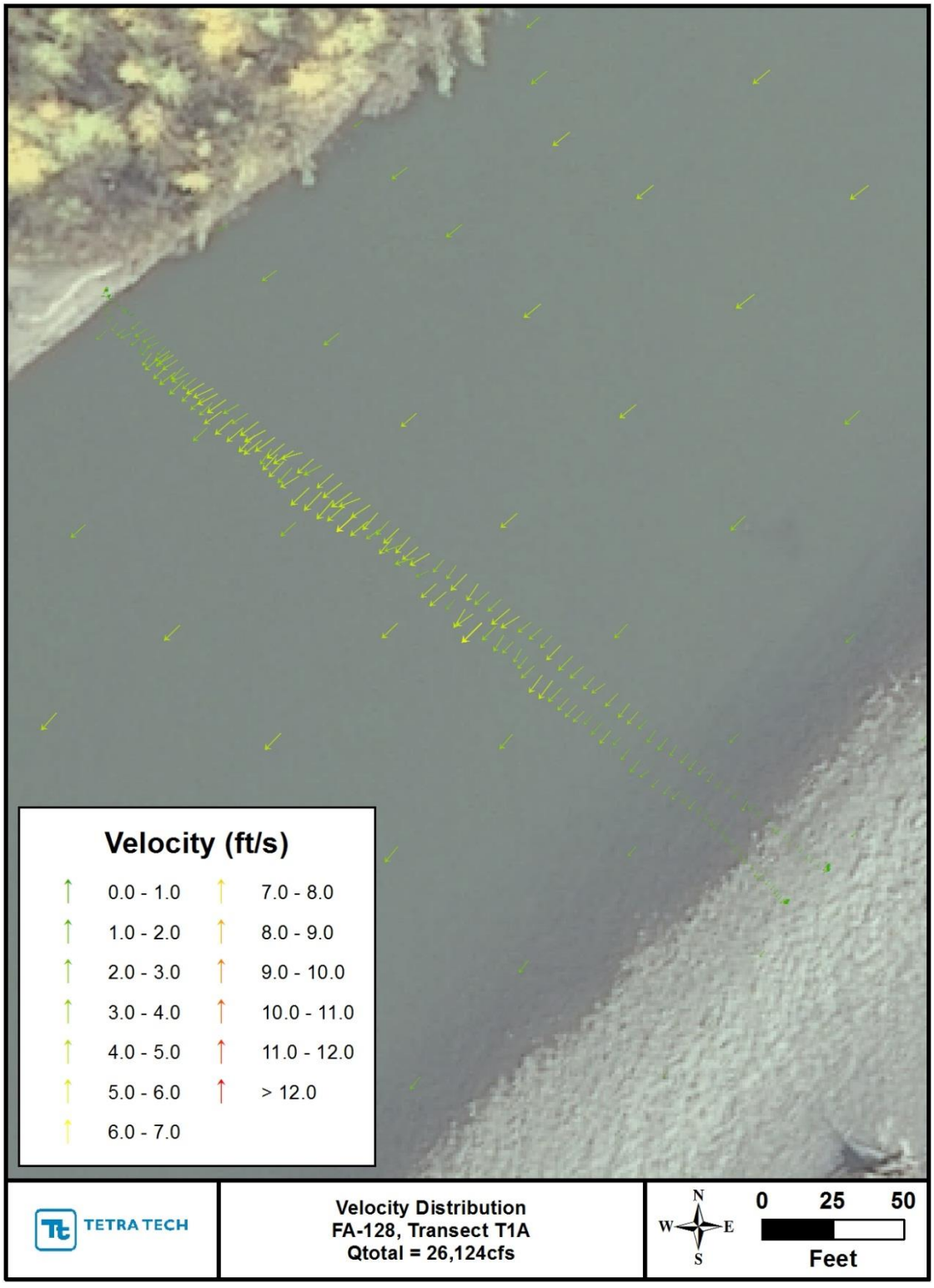

Figure 2.3-19. Comparison of measured and predicted velocity magnitude and direction at Transect 1A (Figure 2.2-7) at 26,184 cfs (Sept. 10, 2013).

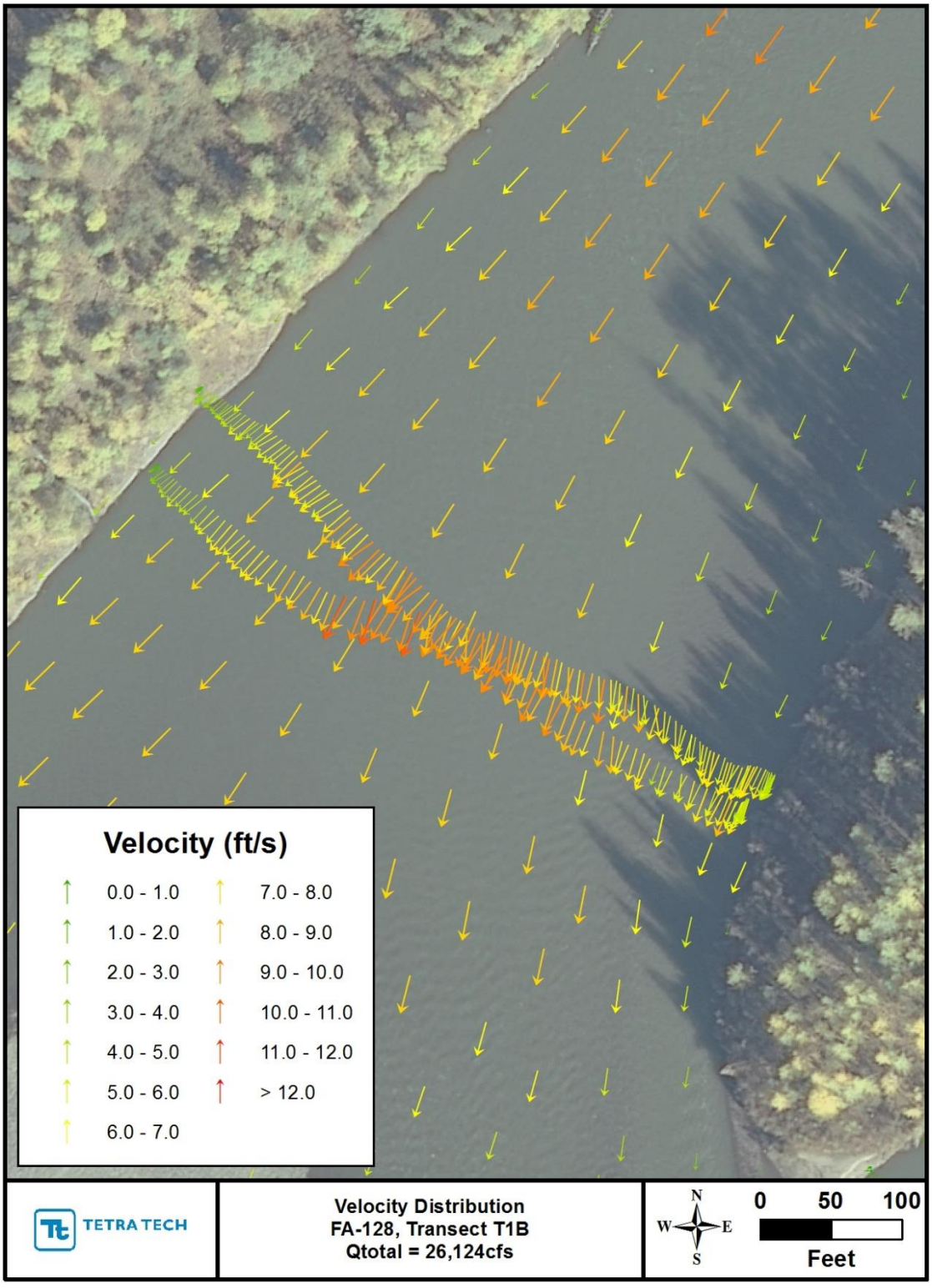

Figure 2.3-20. Comparison of measured and predicted velocity magnitude and direction at Transect 1B (Figure 2.2-7) at 26,184 cfs (Sept. 10, 2013).

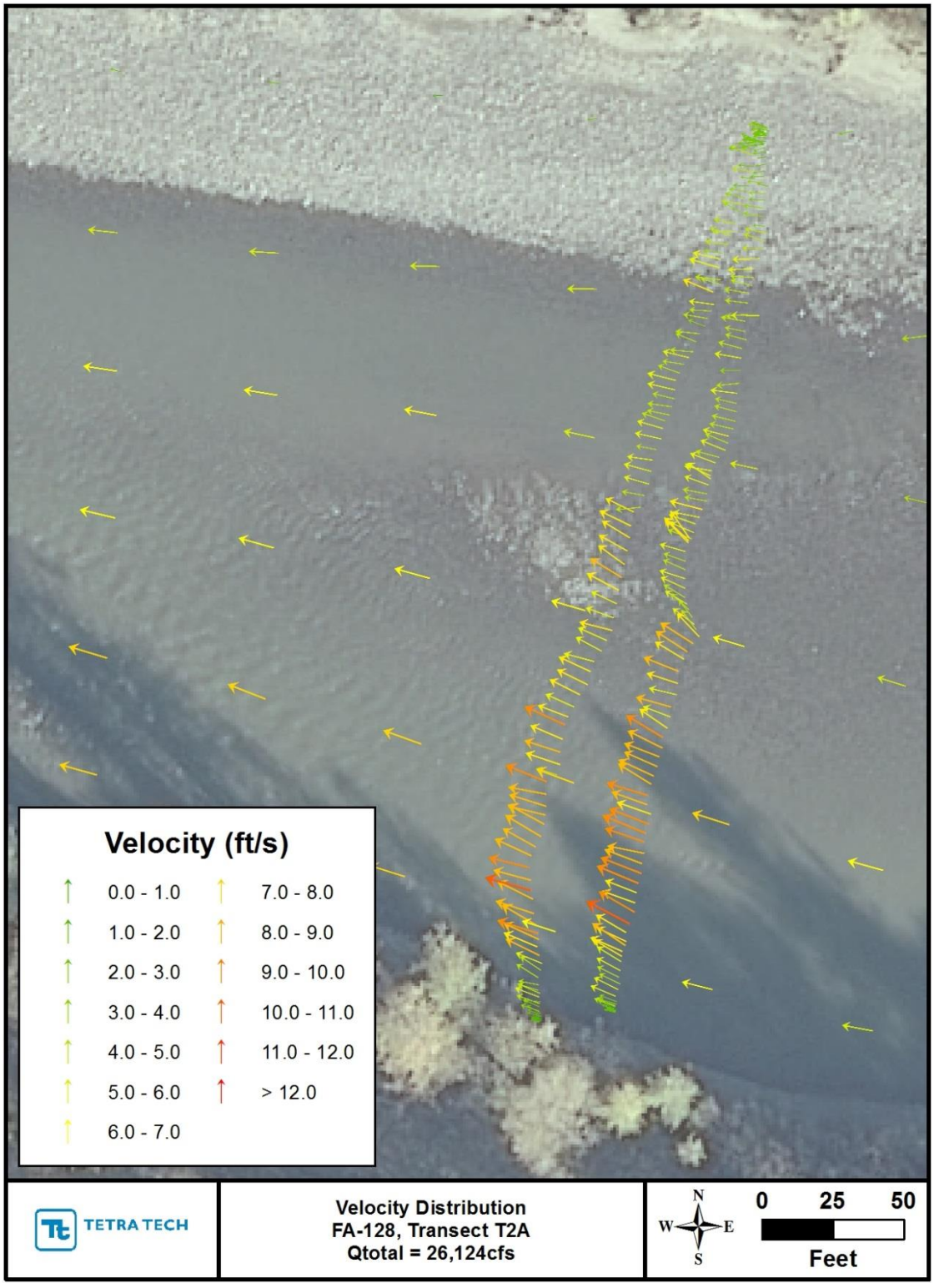

Figure 2.3-21. Comparison of measured and predicted velocity magnitude and direction at Transect 2A (Figure 2.2-7) at 26,184 cfs (Sept. 10, 2013).

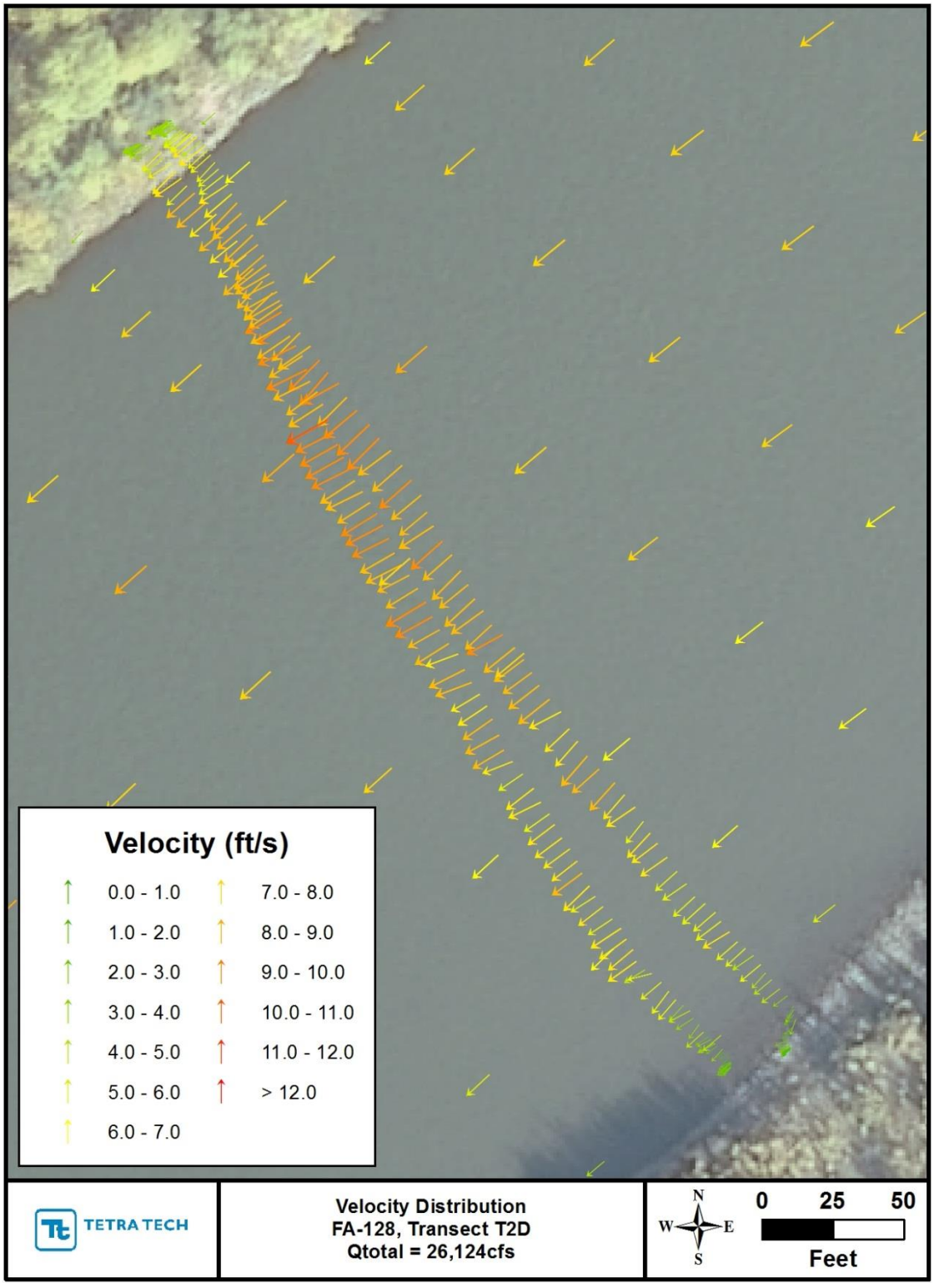

Figure 2.3-22. Comparison of measured and predicted velocity magnitude and direction at Transect 2D (Figure 2.2-7) at 26,184 cfs (Sept. 10, 2013).

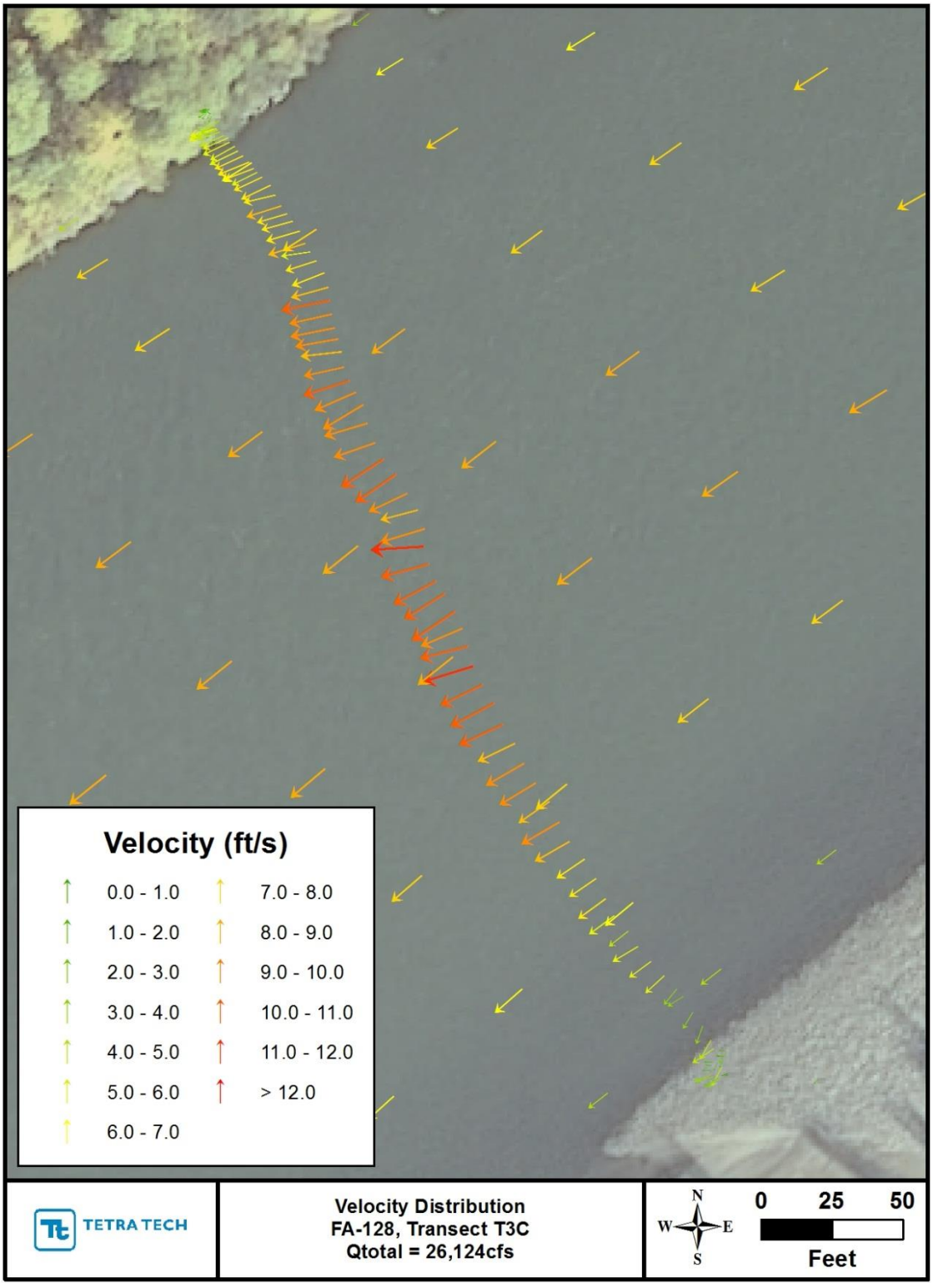

Figure 2.3-23. Comparison of measured and predicted velocity magnitude and direction at Transect 3C (Figure 2.2-7) at 26,184 cfs (Sept. 10, 2013).

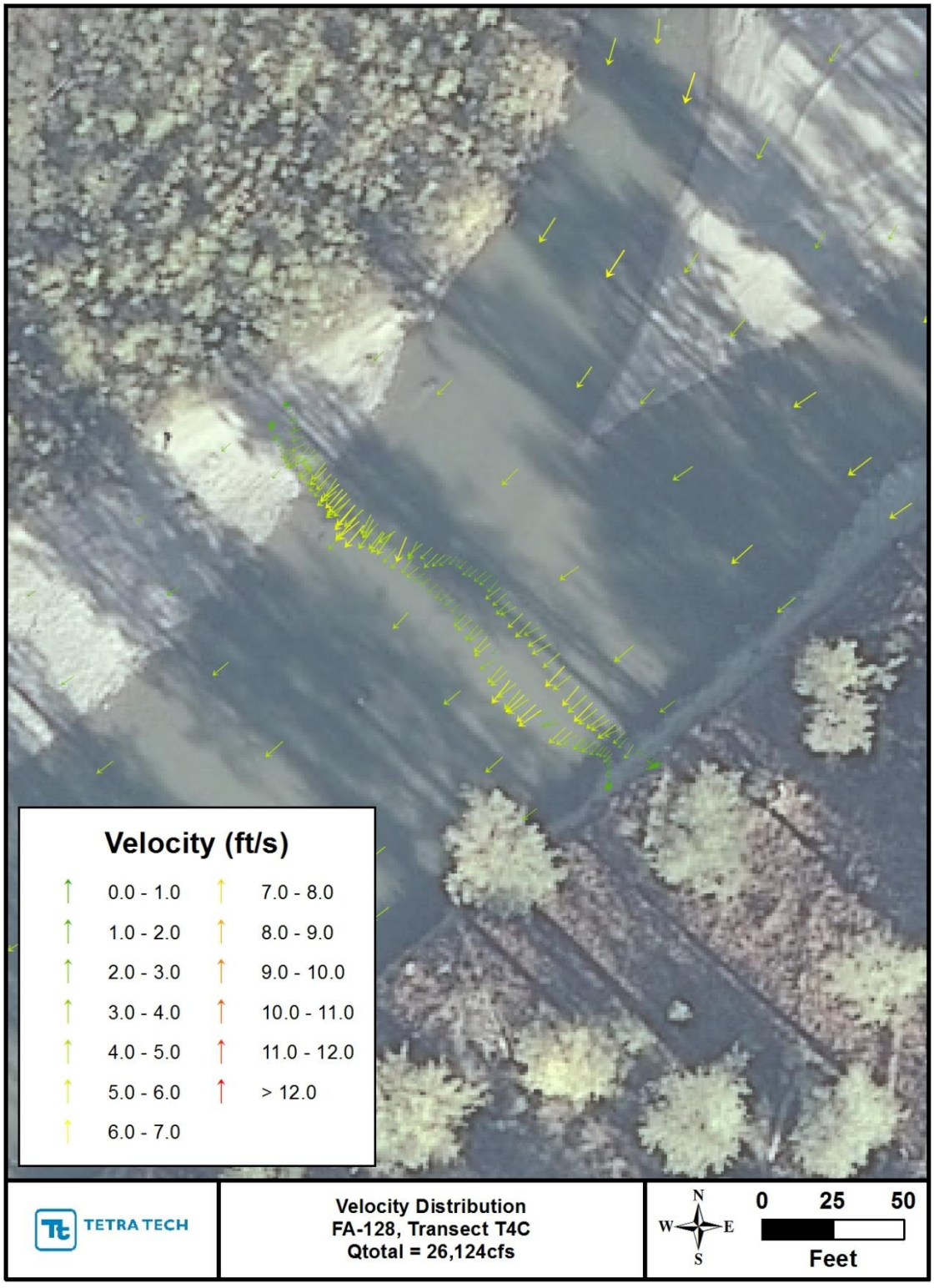

Figure 2.3-24. Comparison of measured and predicted velocity magnitude and direction at Transect 4C (Figure 2.2-7) at 26,184 cfs (Sept. 10, 2013).

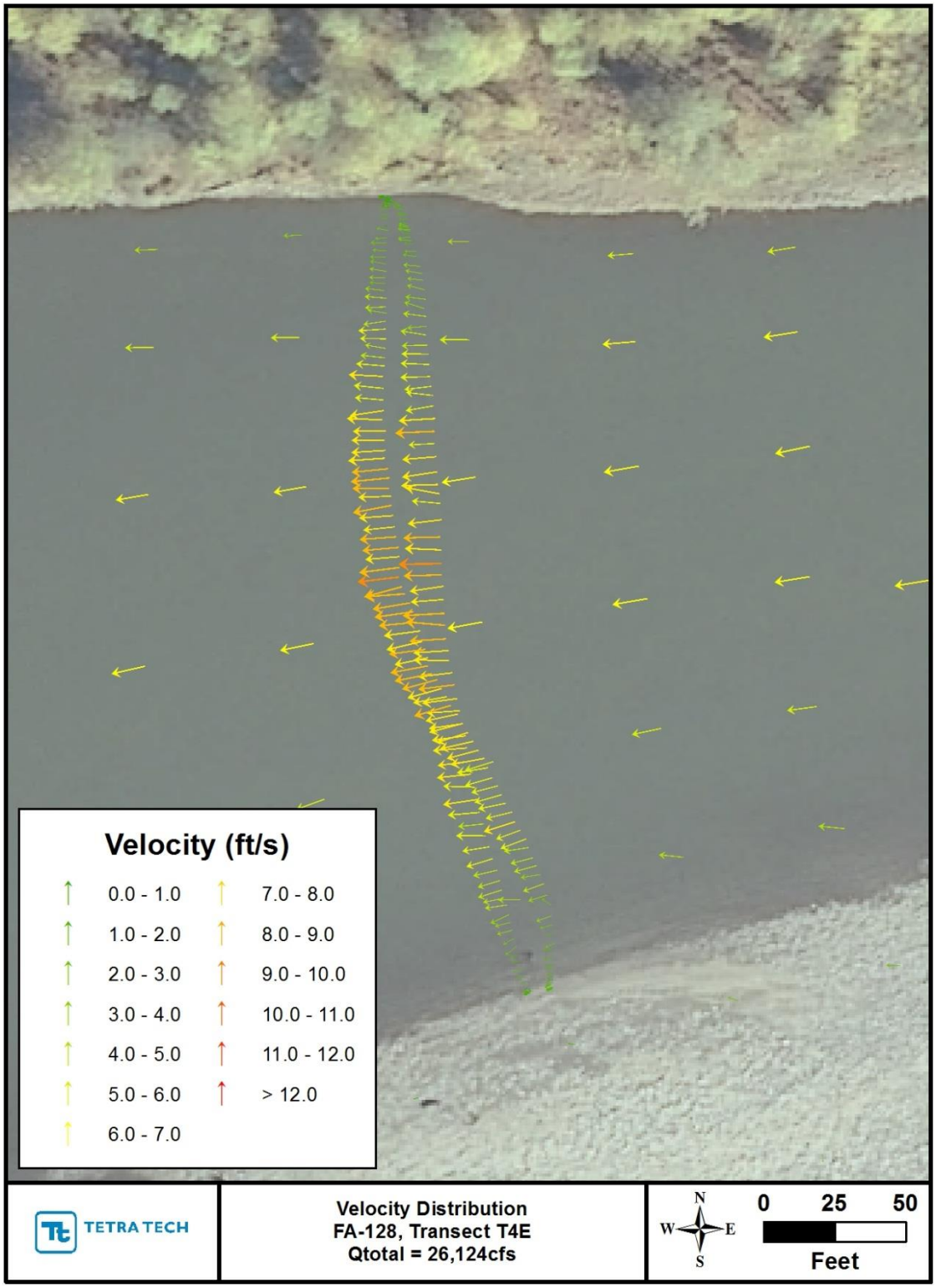

Figure 2.3-25.Comparison of measured and predicted velocity magnitude and direction at Transect 4E (Figure 2.2-7) at 26,184 cfs (Sept. 10, 2013).

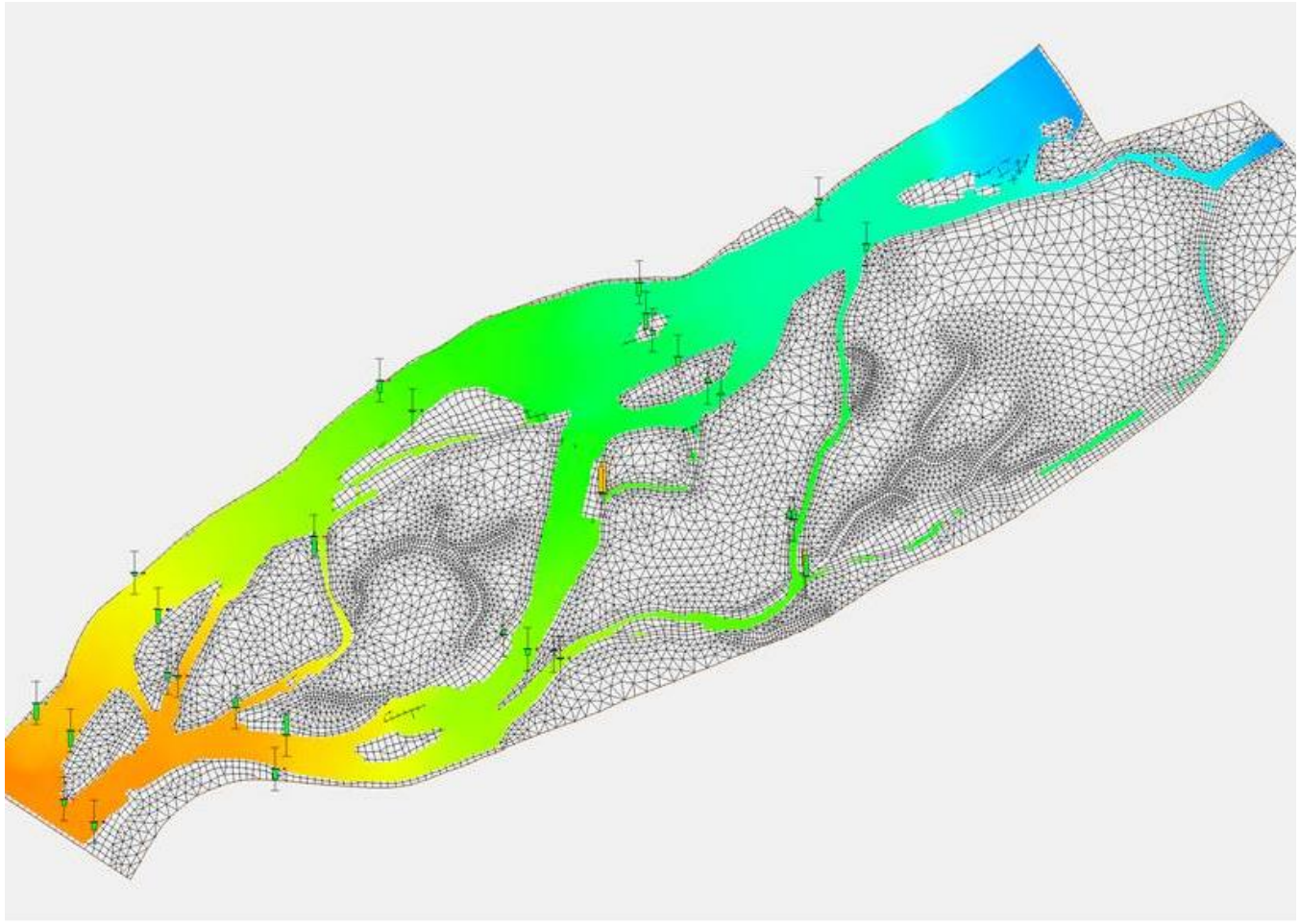

Figure 2.3-26. Screen capture from SMS showing differences between the measured and predicted water-surface elevations from the hydraulic model at 24,705 cfs (July 2, 2013).

The bars indicate the relative differences in water-surface elevations in the direction of the error. For example, if the color is in the lower half, then the predicted water-surface elevation is lower than the measured values. Green bars indicate differences of less than 0.5 feet, and orange bars indicated differences between 0.5 and 1 foot.

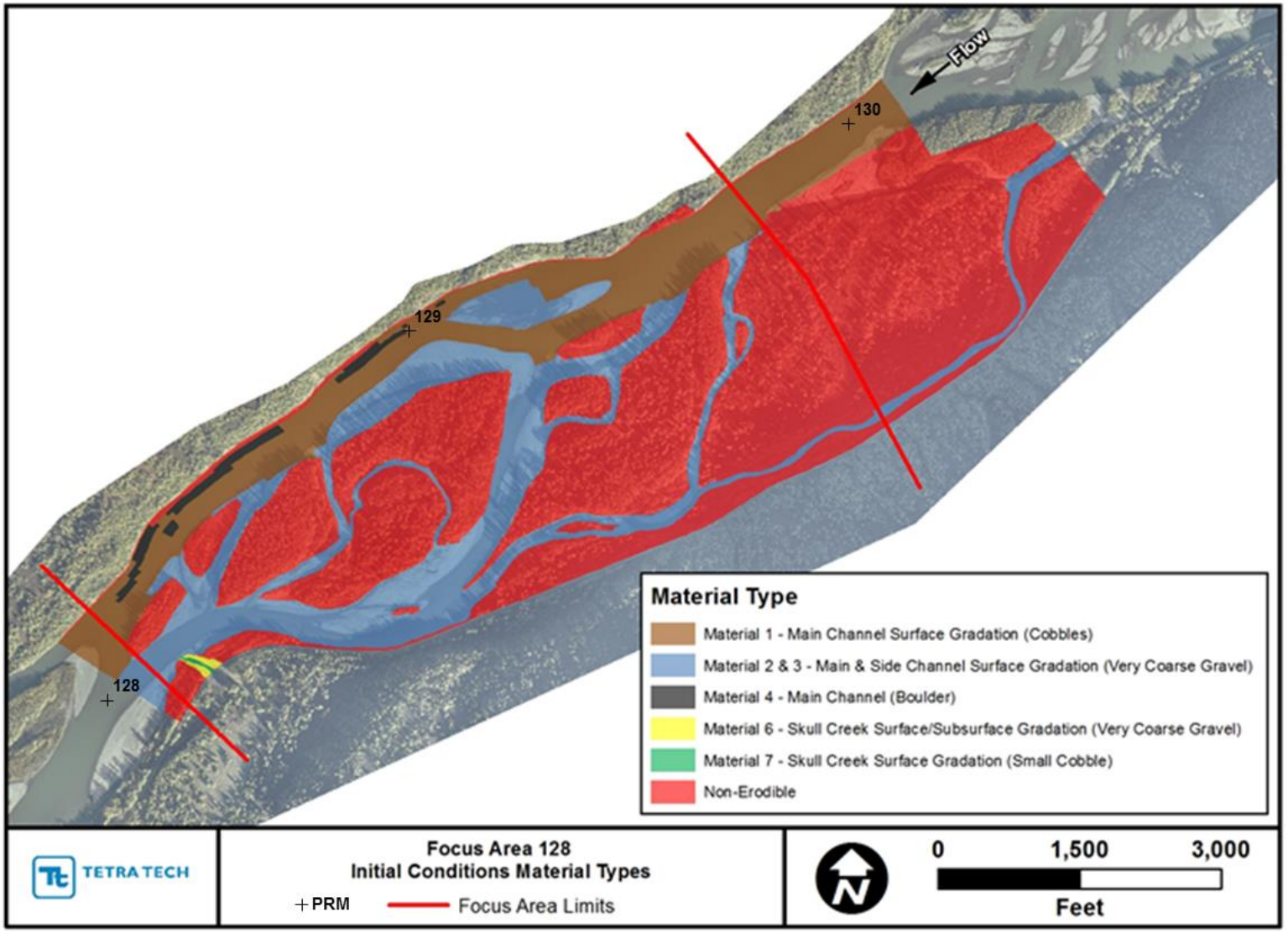

Figure 3.1-1. Representative surface bed materials.

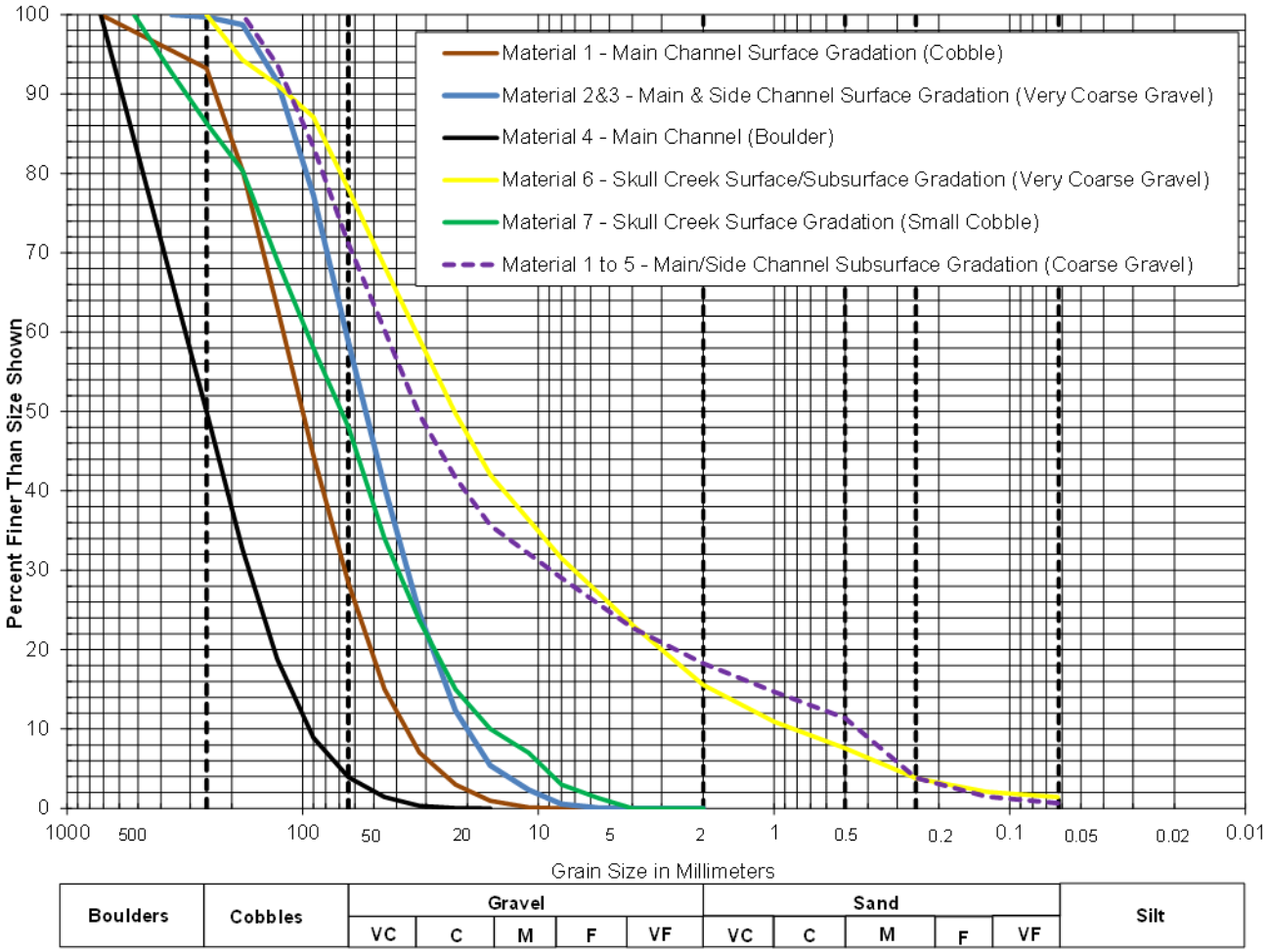

Figure 3.1-2. Representative bed-material gradations applied to the 2-D sediment-transport model.

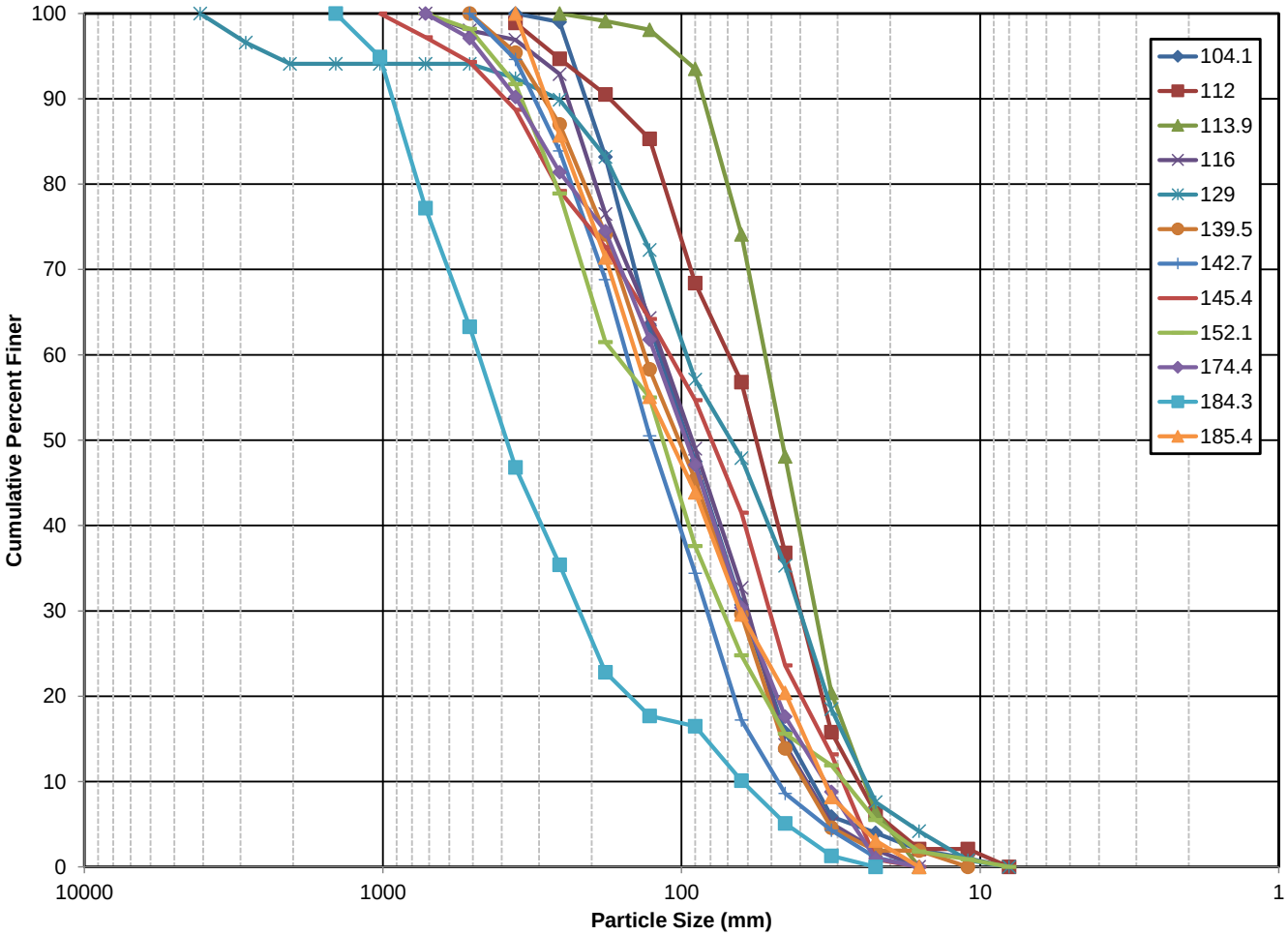

Figure 3.1-3. Sediment gradation curves developed from the winter bed-material sampling (Tetra Tech, 2014b). A median (D_{50}) bed-material size of 100 mm was used to represent Material Type 1 in the 2-D sediment-transport model.

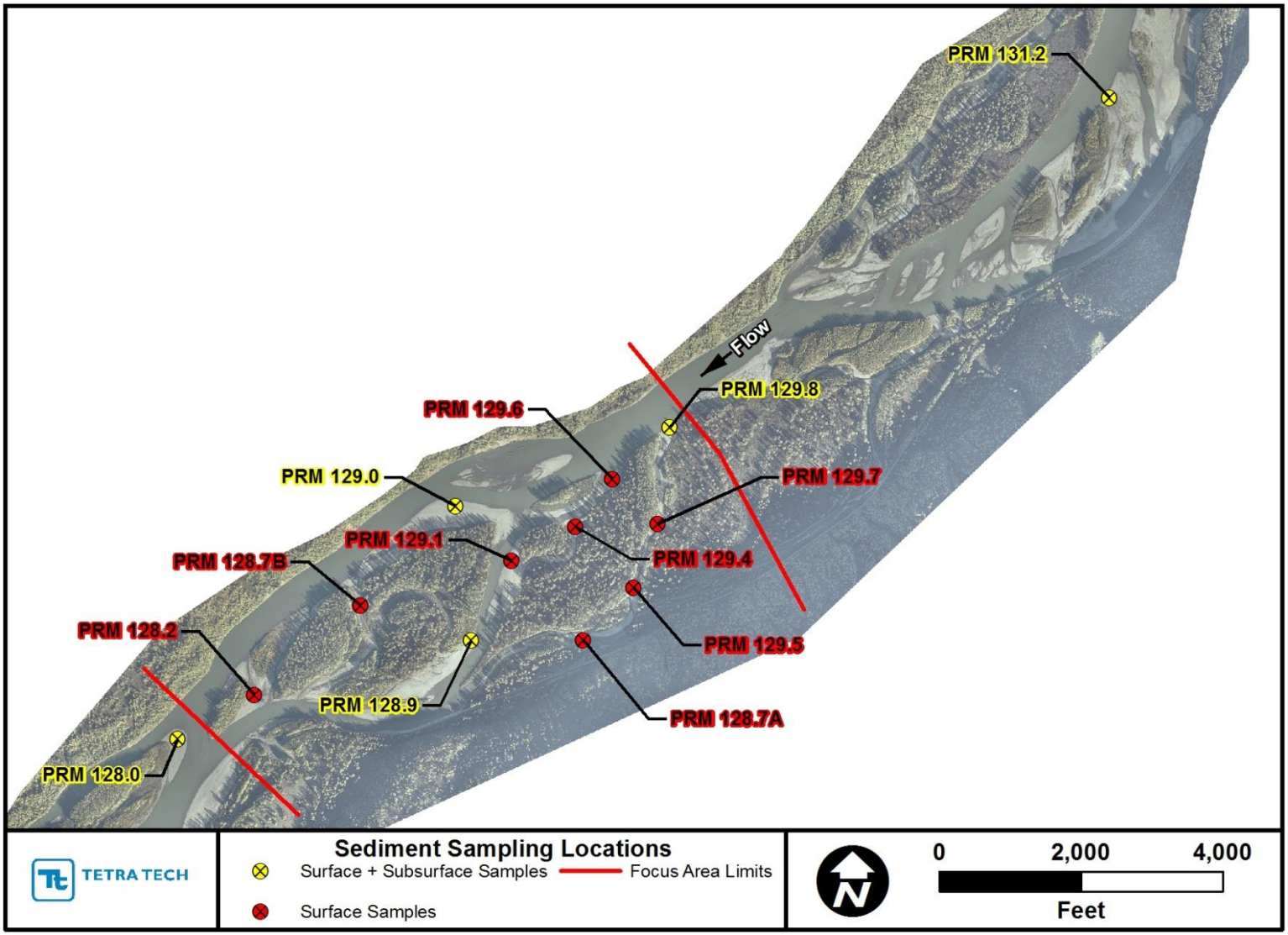

Figure 3.1-4. Location of the sediment samples collected in the vicinity of FA-128.

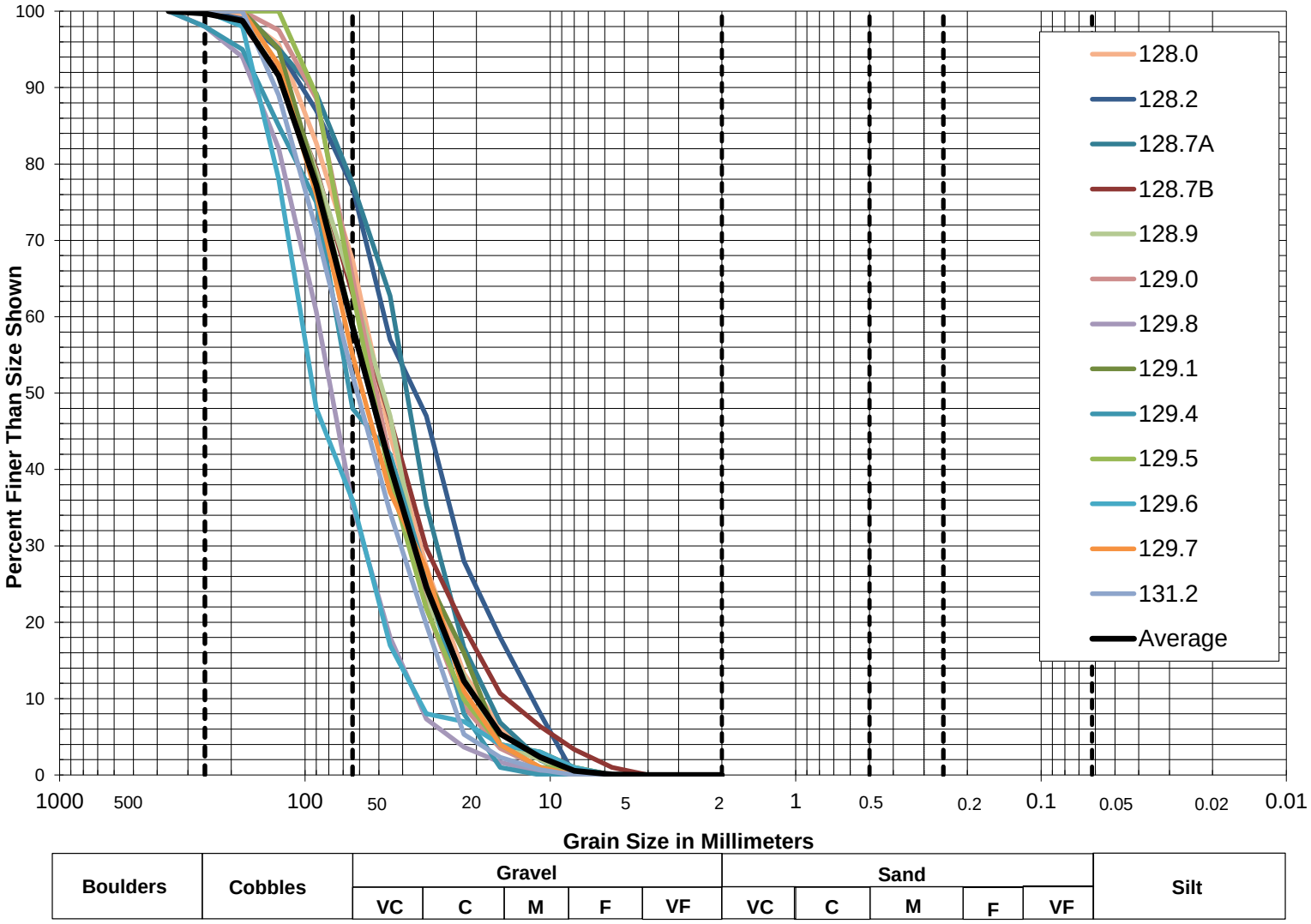

Figure 3.1-5. Bed-material surface gradations collected in the vicinity of FA-128.

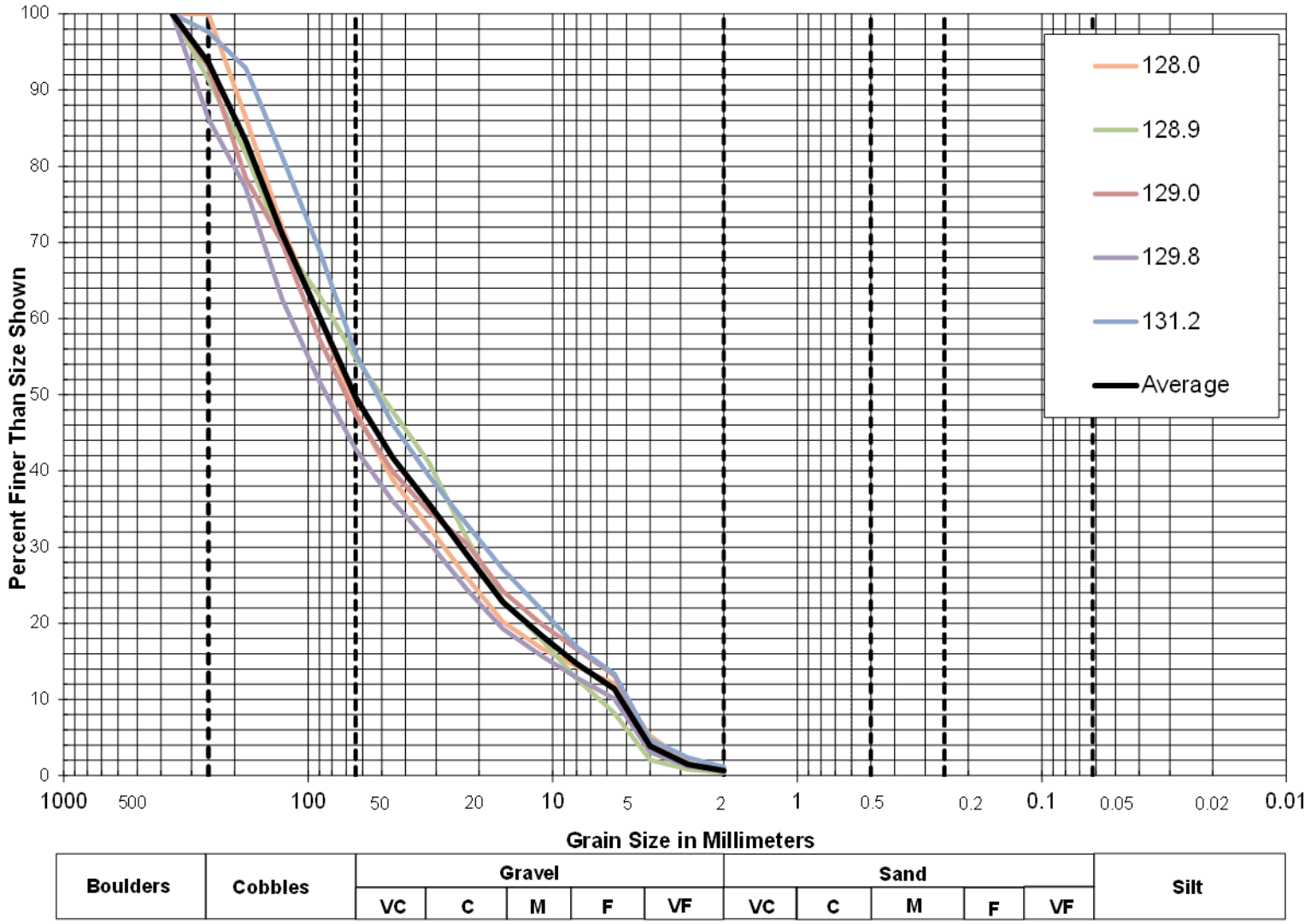

Figure 3.1-6. Bed-material sub-surface gradations collected in the vicinity of FA-128.

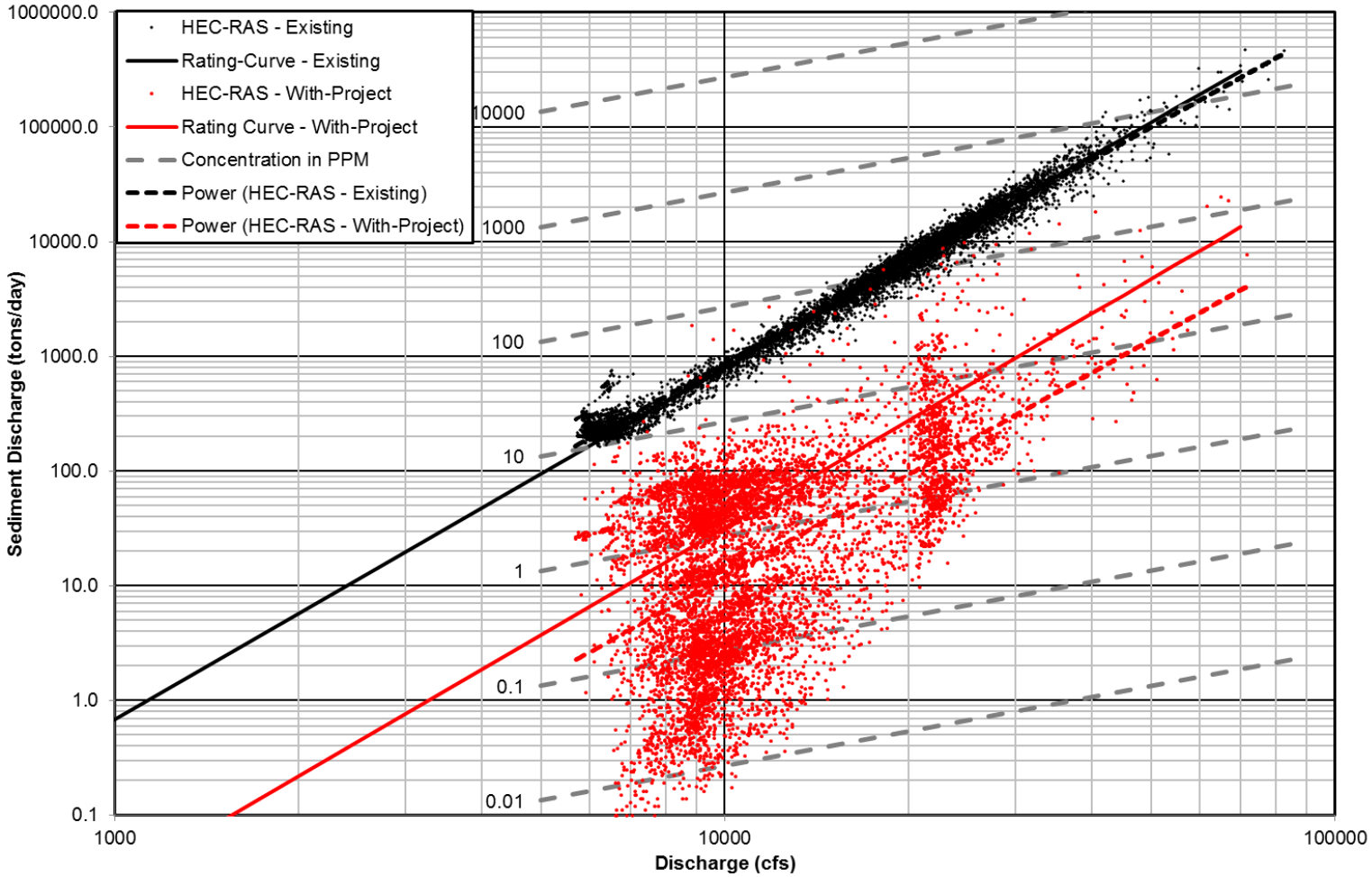

Figure 3.2-1. Comparison of the developed sediment rating curves, best-fit regression line, and the predicted sediment-transport rates from the 1-D model (HEC-RAS) model for the existing and with-Project conditions.

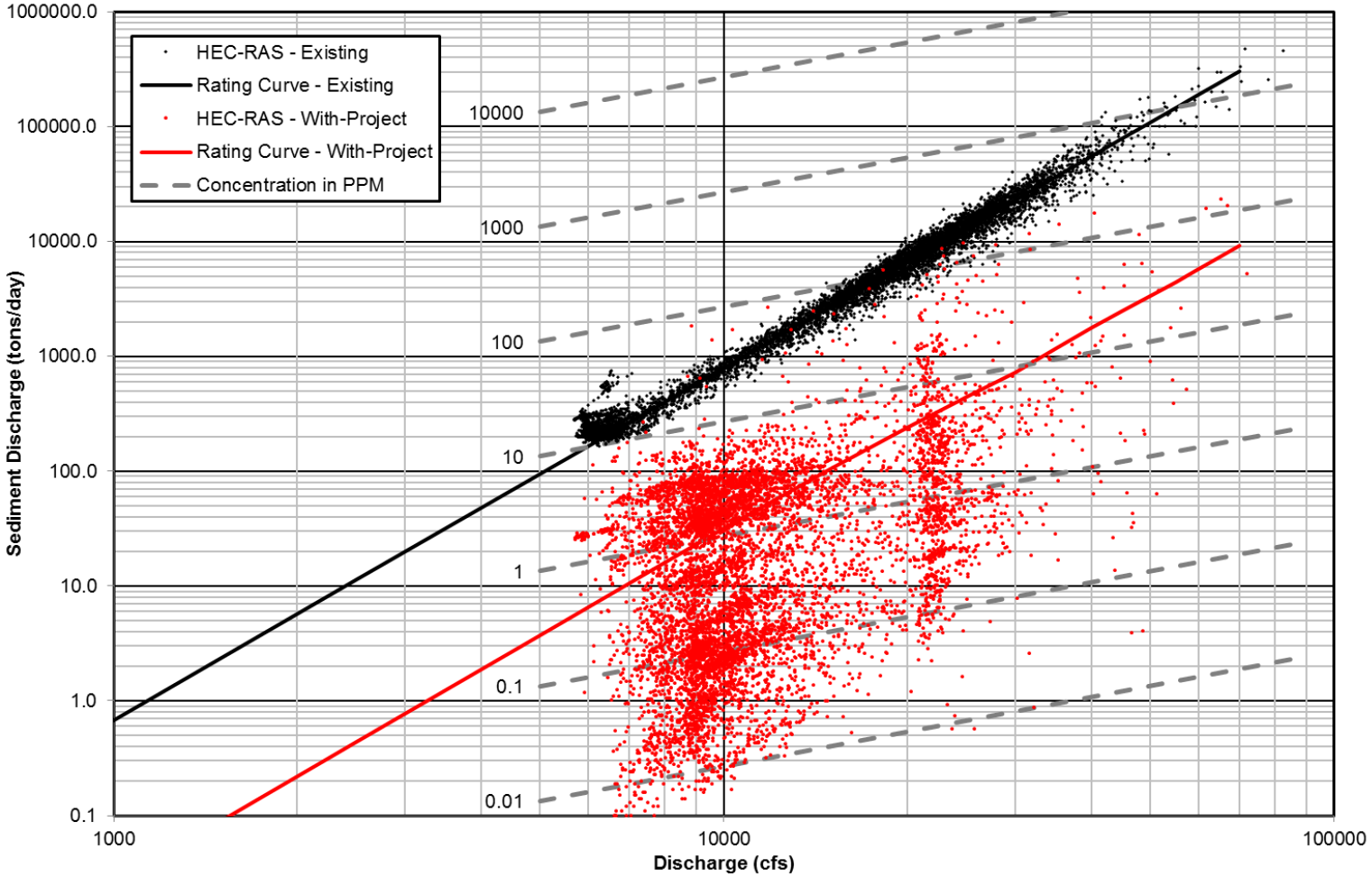

Figure 3.2-2. Comparison between the existing and with-Project sediment-transport rating curves and the HEC-RAS output for sand load (<2 mm).

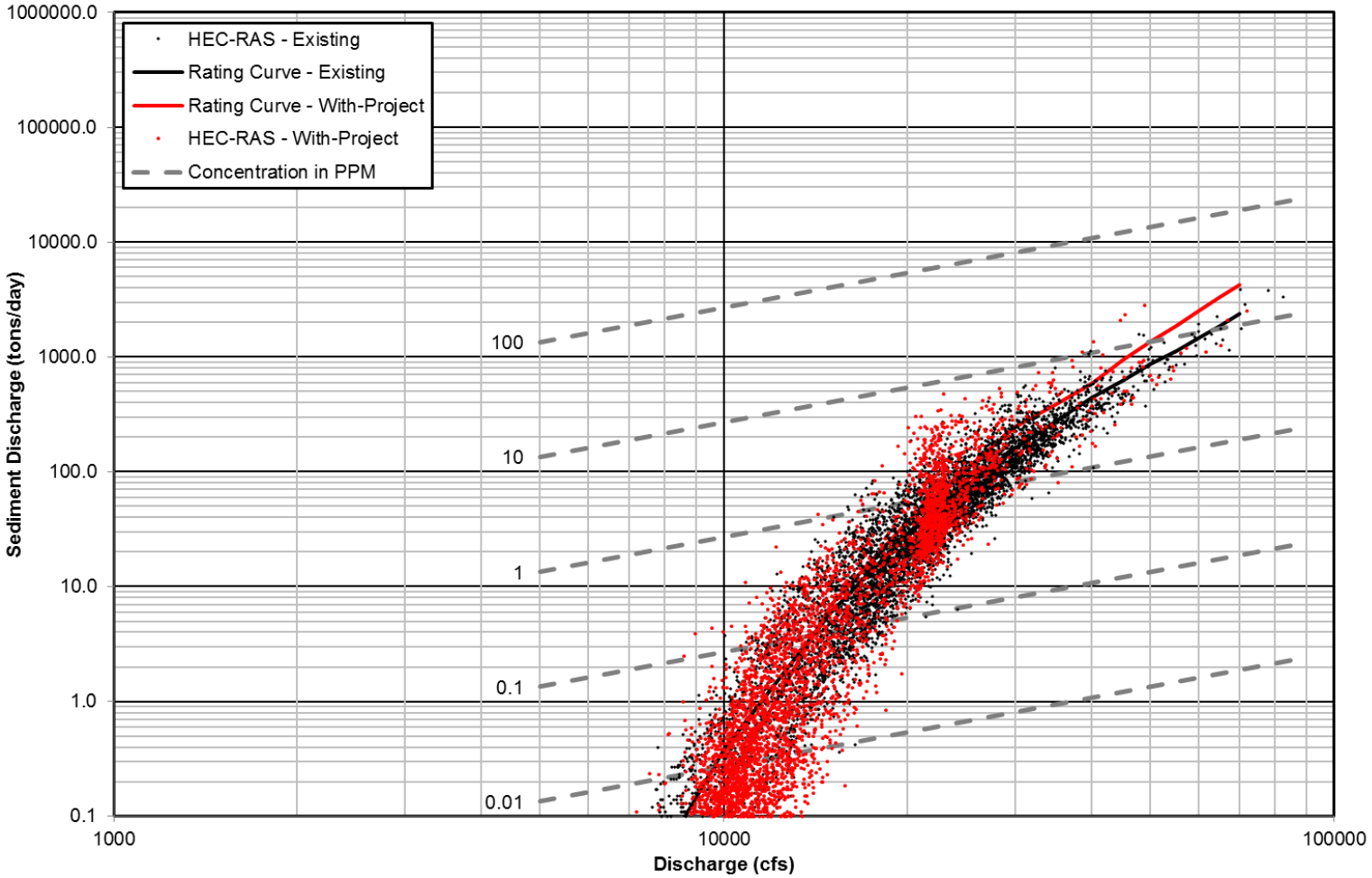

Figure 3.2-3. Comparison between the existing and with-Project sediment-transport rating curves and the HEC-RAS output for gravel load (>2 mm).

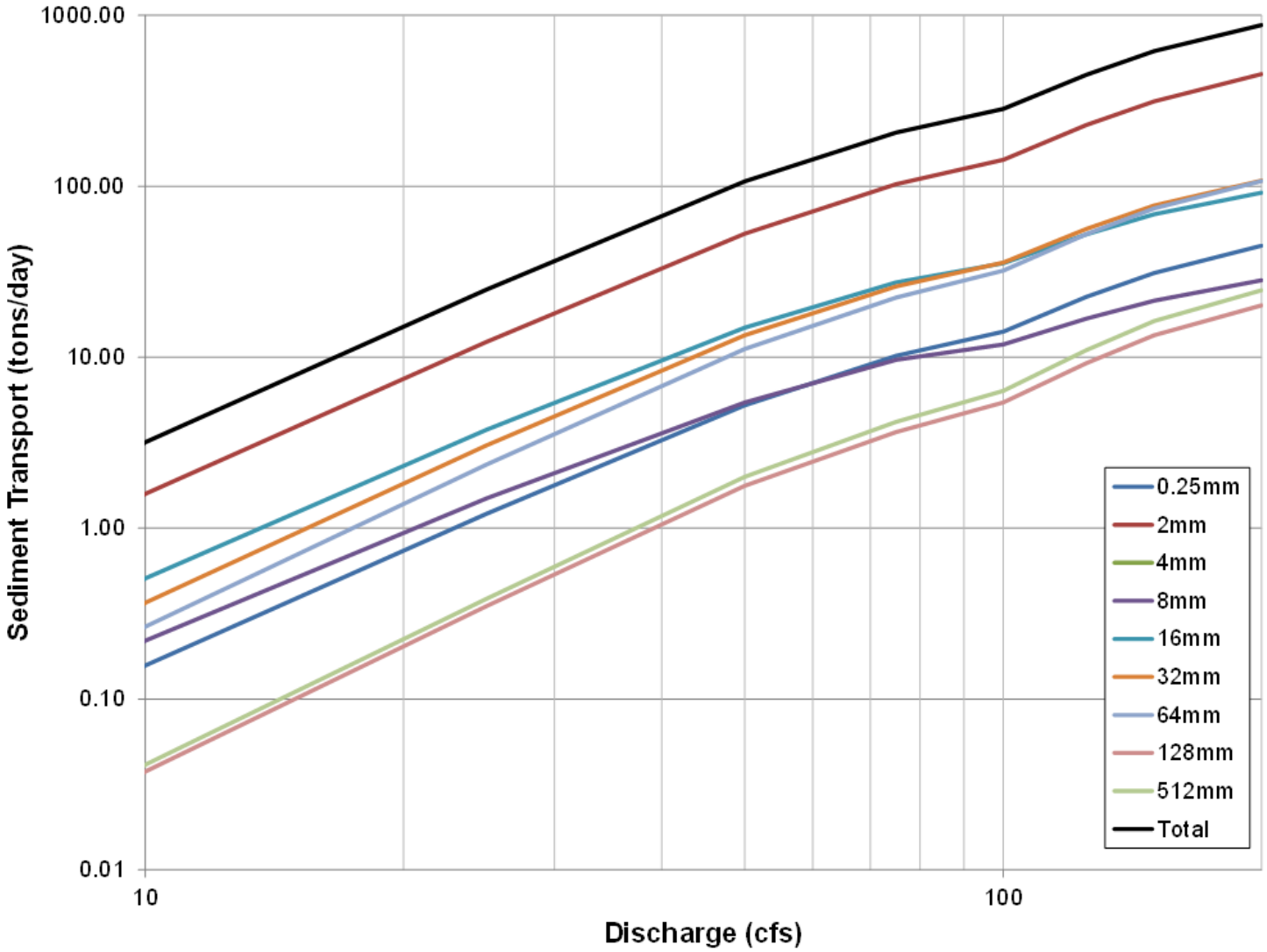

Figure 3.2-4. Comparison of the predicted sediment-transport rating curves for Skull Creek for each size class

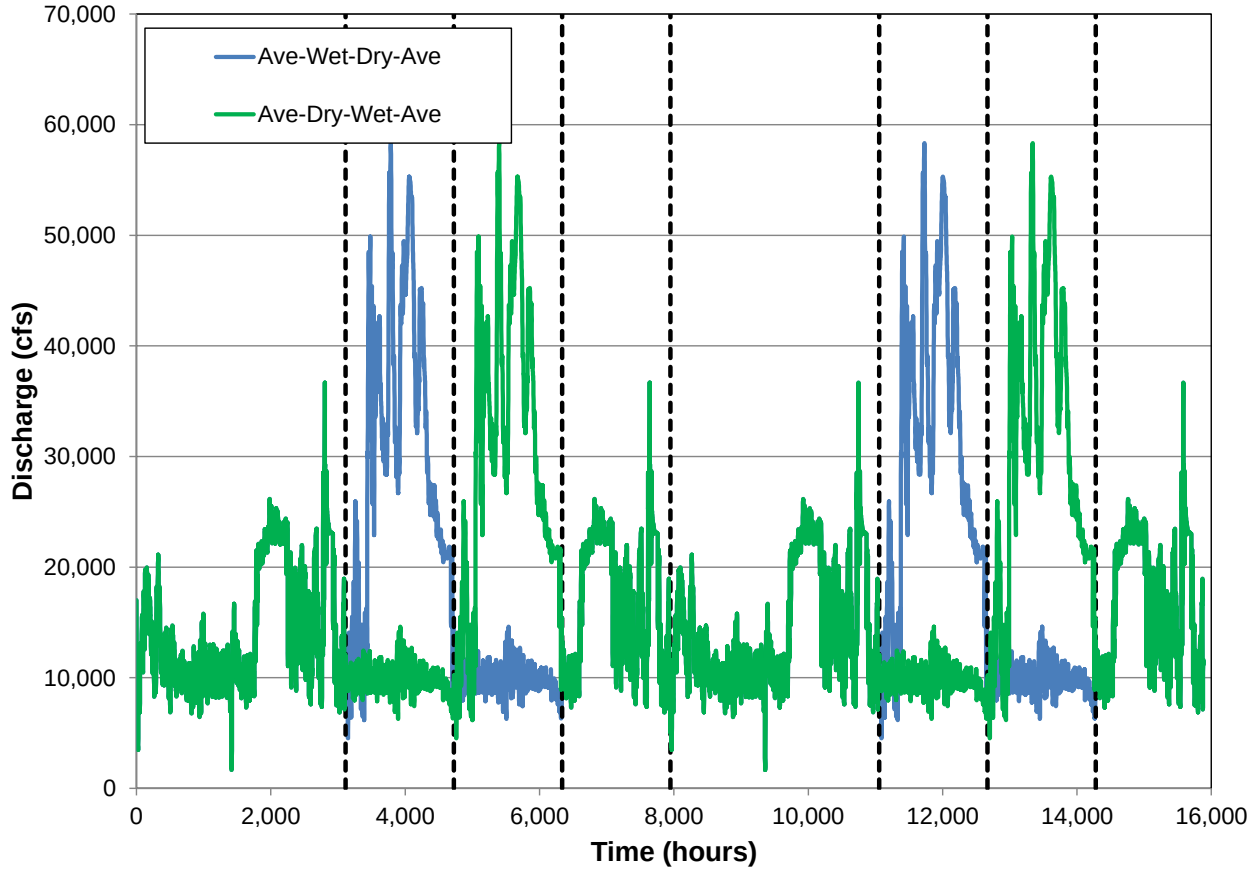

Figure 3.3-1. Hydrographs developed to represent for the 8-year sediment-transport simulations. The 8-year period repeats the Average-Wet/Dry-Average sequence.